Metabolic competition between lipid metabolism and histone methylation regulates sexual differentiation in human malaria parasites.

Chantal T. Harris[1,2], Xinran Tong[1,3], Riward Campelo[1], Inês M. Marreiros[4,5], Leen N. Vanheer[1], Navid Nahiyaan[6], Vanessa A. Zuzarte-Luís[4], Kirk W. Deitsch[1], Maria M. Mota[4], Kyu Y. Rhee[1,6], Björn F.C. Kafsack[1*]

[1] Department of Microbiology & Immunology, Weill Cornell Medicine, New York, USA.
[2] Immunology & Microbial Pathogenesis Graduate Program, Weill Cornell Medicine, New York, USA.
[3] BCMB Allied Graduate Program, Weill Cornell Medicine, New York, NY 10065, USA.
[4] Instituto de Medicina Molecular João Lobo Antunes, Faculdade de Medicina Universidade de Lisboa, Lisbon, Portugal.
[5] Instituto de Ciências Biomédicas Abel Salazar (ICBAS), Universidade do Porto, Porto, Portugal.
[6] Division of Infectious Diseases, Weill Department of Medicine, Weill Cornell Medicine, New York, USA.

* Please send correspondence to bjk2007@med.cornell.edu

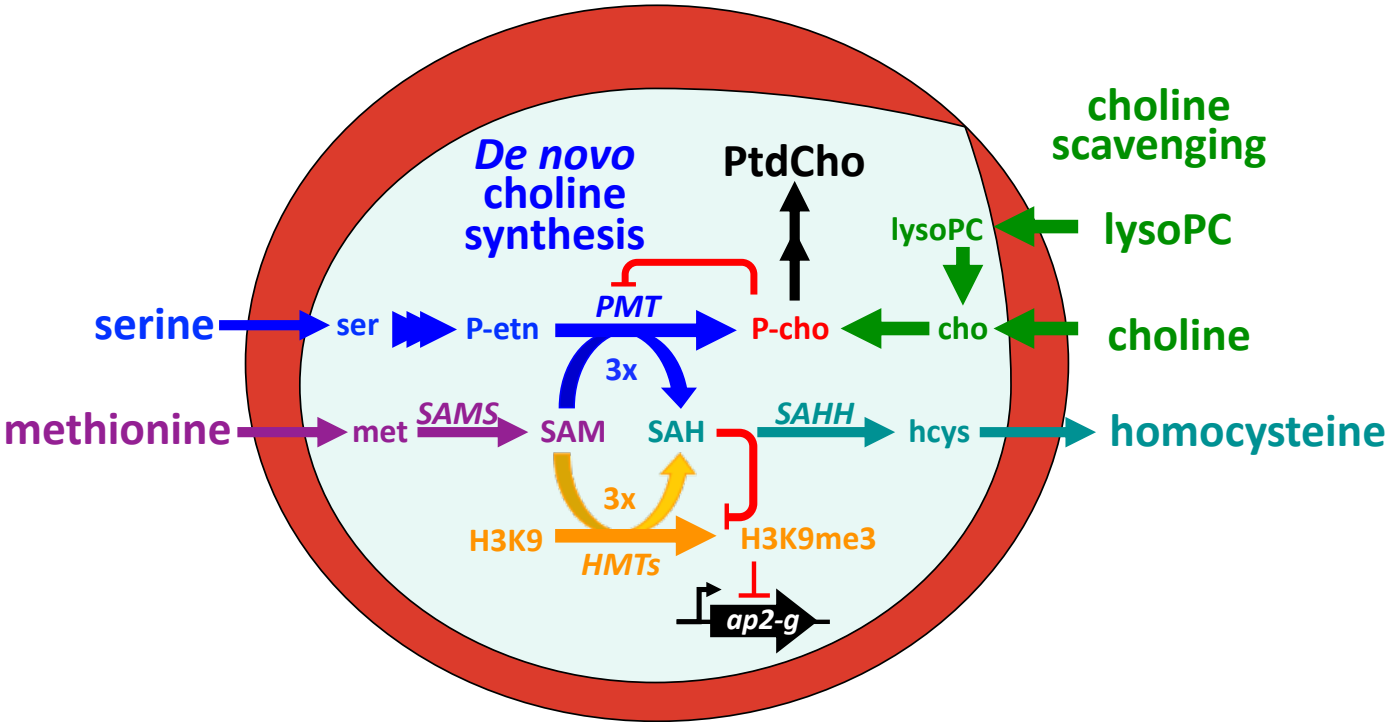

ABSTRACT

For *Plasmodium falciparum*, the most widespread and virulent human malaria parasite, persistence depends on continuous asexual replication in red blood cells, while transmission requires their differentiation into non-replicating gametocytes that can infect the mosquito vector. This decision is controlled by stochastic derepression of a heterochromatin-silenced locus encoding *Pf*AP2-G, the master transcription factor of sexual differentiation. The frequency of *pfap2-g* derepression was shown to be responsive to extracellular phospholipid precursors but the mechanism linking these metabolites to epigenetic regulation of *pfap2-g* was unknown. Here we show that this response is mediated by metabolic competition for S-adenosylmethionine between histone methyltransferases and phosphoethanolamine methyltransferase, a critical enzyme in the parasite's pathway for *de novo* phosphatidylcholine synthesis. When phosphatidylcholine precursors are scarce, increased consumption of SAM for de novo phosphatidylcholine synthesis impairs maintenance of the histone methylation responsible for silencing *pfap2-g,* increasing the frequency of derepression and sexual differentiation.

KEYWORDS

malaria; *Plasmodium falciparum*; differentiation; metabolism; chromatin; metabolic epigenome; methylation;

ABBREVIATIONS

3-DZA: 3-deaza-adenosine; *cho*: choline; *CDP-cho*: cytidine diphosphate-choline; *GlcNAC:* N-acetyl glucosamine; *Glm*: glucosamine; *hcys*: homocysteine; *iRBC*: infected *RBC*; *LysoPC*: lyso-phosphatidylcholine; *met*: methionine; *P-cho*: phospho-choline; *P-etn*: phospho-ethanolamine; *P-etn-me1/2*: mono/di-methylphosphoethanolamine; *PMT*: phosphoethanolamine methyltransferase; *PtdCho*: phosphatidylcholine; *RBC*: red blood cell; *SAH*: S-adenosylhomocysteine; *SAHH*: S-adenosylhomocysteine hydrolase; *SAM*: S-adenosylmethionine; *SAMS*: S-adenosylmethionine synthetase; *ser*: serine; *TMP*: trimethoprim; *uRBC*: uninfected RBC.

INTRODUCTION

Transmission of malaria parasites requires differentiation from replicating asexual blood-stream forms that are responsible for pathogenesis into non-replicating sexual stages, called gametocytes, that can infect the mosquito vector. Parasite success depends on a careful balance between asexual replication, to maintain human infection, and gametocyte formation, to infect the mosquito vector for further transmission. The regulation of this balance is key to understanding the dynamics of malaria pathogenesis and transmission (Drakeley et al., 2006). Developmental commitment to sexual differentiation requires expression of the transcription factor AP2-G (Kafsack et al., 2014; Sinha et al., 2014). This requires the transcriptional activation of the *ap2-g* locus, which is actively silenced in a heterochromatin-dependent manner during asexual replication (Brancucci et al., 2014a; Fraschka et al., 2018; Kafsack et al., 2014; Lopez-Rubio et al., 2009). The frequency of sexual differentiation relies on the efficiency of heterochromatin maintenance at the *ap2-g* locus, which depends on the efficient trimethylation of lysine 9 on histone H3 of newly placed nucleosomes and recognition of this mark by heterochromatin protein 1 (Brancucci et al., 2014b; Coleman et al., 2014; Filarsky et al., 2018; Kafsack et al., 2014). So long as *ap2-g* remains efficiently silenced, parasites continue replicating asexually. However, when heterochromatin maintenance at this locus is impaired, low-level AP2-G expression can activate a transcriptional feedback loop when the transcription factor binds motifs upstream of its own locus, upregulating its transcription. This drives AP2-G expression to high levels and activates the transcriptional program underlying gametocytogenesis (Josling et al., 2020; Kafsack et al., 2014; Kent et al., 2018; Llorà-Batlle et al., 2020; Poran et al., 2017).

In the laboratory, the frequency of sexual commitment of *Plasmodium falciparum*, the most wide-spread and virulent human malaria parasite, varies from less than 1% to greater than 40% in response to culture conditions, including parasite density and media composition (Neveu et al., 2020a). Recent work showed that lysophosphatidylcholine (LysoPC) and choline, precursors of phosphocholine (P-cho), the headgroup required for phosphatidylcholine (PtdCho) synthesis, act as potent suppressors of sexual commitment (Brancucci et al., 2017). This ability of parasites to vary their investment into gametocyte production illustrates the parasites' ability to sense their in-host environment and respond adaptively to resource abundance (Pollitt et al., 2011) or anatomical niche (Joice et al., 2014; Venugopal et al., 2020). However, the underlying mechanisms that link the availability of these metabolites to *pfap2-g* activation remain unknown. Here, we show that the availability of P-cho precursors regulates sexual commitment by shifting the metabolic competition for the methyl donor S-adenosyl methionine (SAM) between the methyltransferase required for *de novo* synthesis of P-cho and the histone methyltransferases maintaining heterochromatin-mediated silencing, including at the *ap2-g* locus.

P-cho precursor availability alters sexual commitment and intracellular concentrations of SAM and SAH.

As the parasite grows during its 48-hour asexual replication cycle, the membrane content of infected red blood cells (iRBCs) increases 8-fold, with PtdCho accounting for more than half of this increase in membrane biomass (Gulati et al., 2015; Wein et al., 2018). In *P. falciparum*, PtdCho is exclusively derived from P-cho, which can be generated *de novo* from serine via phosphoethanolamine (P-etn) or scavenged from extracellular sources, including choline and choline-containing phospholipids such as LysoPC (Kilian et al., 2018) (Figure 1A). When P-cho precursors are available, parasites down-regulate phosphoethanolamine methyltransferase (PMT), which generates P-cho by transferring three consecutive methyl-groups from the methyl-donor S-adenosylmethionine (SAM) onto P-etn (Garg et al., 2015; Kilian et al., 2018).

Consistent with earlier reports (Brancucci et al., 2017), we found that supplementation with exogenous P-cho precursors (see Table S1 for media composition) during a single replication cycle suppressed sexual commitment (Figure 1B-C) and increased the P-cho and CDP-choline levels of iRBCs compared to conditions when these precursors were scarce (Figure 1D-E). As in other eukaryotes (Ye et al., 2017), *de novo* synthesis of PtdCho is also a major consumer of SAM and source of S-adenosyl homocysteine (SAH) in malaria parasite blood-stages. When exogenous P-cho precursors are abundant, levels of SAH decreased significantly in

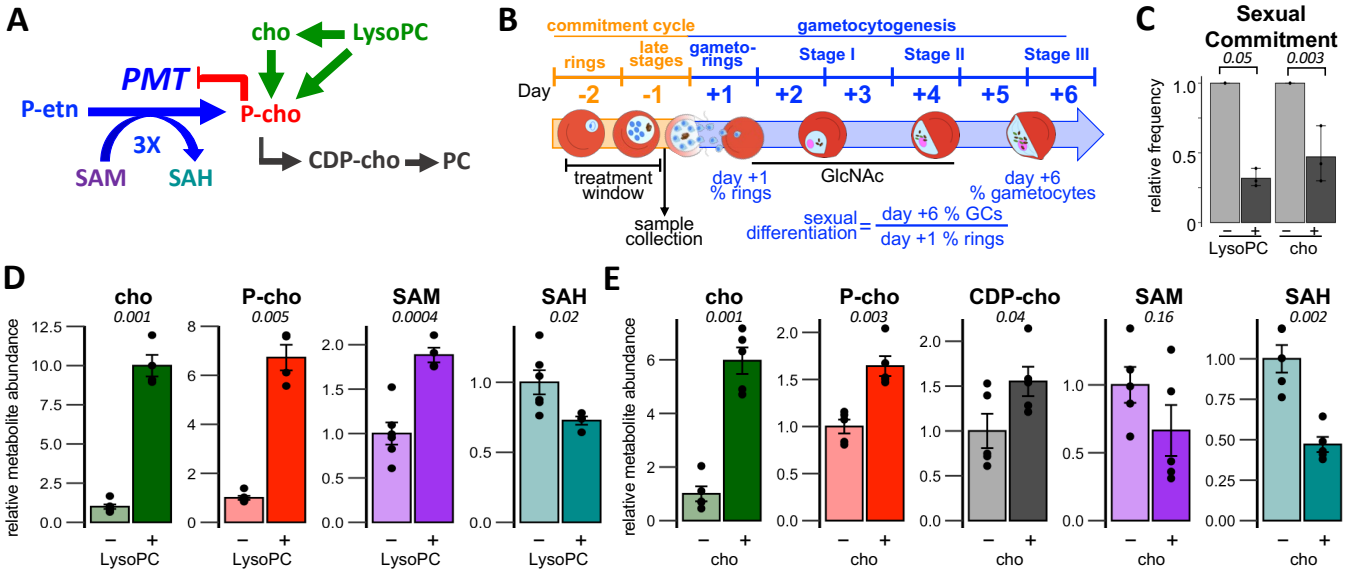

Figure 1. Phosphocholine precursor availability alters parasite SAM and SAH levels. (A) PtdCho (PC) is generated exclusively from P-cho, which can be scavenged from extracellular choline or LysoPC or synthesized de novo via triple methylation of P-etn by PMT, consuming 3 equivalents of SAM and producing 3 equivalents of SAH per P-cho. **(B)** Synchronous blood-stages were grown for a single cycle (commitment cycle) under various nutrient conditions and samples were collected 36 hours post-invasion. Treated parasites were allowed to re-invade and 50 mM N-acetylglucosamine was added on Day +1 to block asexual replication. The sexual differentiation rate is defined as the percentage of Day +1 ring stages that differentiate into stage III gametocytes by Day +6. **(C)** P-cho precursors inhibit the frequency of sexual differentiation (n=3). Italicized numbers are p-values from two-sided paired t-tests. **(D-E)** Intracellular metabolite levels are altered in response to LysoPC or choline supplementation in parasite media. (n=4-6). Bar graphs indicates the mean values relative to the reference condition ± s.e.m. Italicized numbers are p-values from two-sided t-tests.

response to both LysoPC and choline supplementation compared to conditions requiring greater de novo synthesis of P-cho from P-etn (Figure 1D-E). SAM levels increased in response to LysoPC but remained unchanged upon choline supplementation. One possibility for this difference is the additional energetic cost associated with scavenging choline, which must be phosphorylated using ATP, while LysoPC can be cleaved directly into P-cho by phospholipase C. This is supported by the observation that the suppressive effects of choline supplementation can be reversed by reducing the availability of glucose in the growth medium (Brancucci et al., 2017). This metabolic response to P-cho precursors is dose dependent (Figure S1) indicating that P-cho precursor availability regulates intracellular levels of SAM and SAH. These changes in the intracellular abundances of P-cho, SAM, and SAH were limited to iRBCs and absent from uninfected RBCs (Figure S2).

***Pf*PMT activity drives changes in intracellular levels of SAM and SAH.** Parasites down-regulate *pfpmt* (Witola and Ben Mamoun, 2007), as indicated by the decreases in the *pfpmt* transcript abundance (Figure 2A) and the levels of the mono- and di-methylated P-etn reaction intermediates (Figure 2B), when P-cho precursors can be scavenged into P-cho and CDP-cho (Figure 2B). The effect of *Pf*PMT activity on intracellular SAM and SAH levels is unknown but if P-cho synthesis by *Pf*PMT is a major metabolic sink of SAM and source of SAH, their levels should track *Pf*PMT abundance and activity inversely. We therefore measured the effect of *pfpmt* ablation (Witola et al., 2008) on the abundance of these metabolites. Indeed, loss of *pfpmt* resulted in a nearly 5-fold increase in SAM when compared to wild-type parasites while SAH levels fell below the level of detection (Figure 2C). Intriguingly, a near complete suppression of gametocytogenesis had previously been reported in *pfpmt* knockout parasites that was restored to parental levels upon genetic complementation (Bobenchik et al., 2013; Witola et al., 2008). Genetic complementation also restored SAM to wild-type levels and increased SAH substantially. These data strongly suggest that *Pf*PMT activity is a significant regulator of intracellular SAM/SAH levels, as well as gametocytogenesis.

To confirm this connection between *Pf*PMT activity, SAM metabolism and sexual commitment, we generated inducible *pfpmt* knockdown parasites by inserting the glucosamine-responsive autocatalytic *glmS* ribozyme into the endogenous *pfpmt* 3'UTR (Prommana et al., 2013) (Figure S3). Treatment of *pfpmt-glmS* cultures with glucosamine during the commitment cycle reduced *Pf*PMT protein levels by 55% (Figure 2D), resulting in a 2-fold increase in intracellular SAM and significantly suppressed sexual commitment, even in the absence of P-cho precursors (Figure 2E-F).

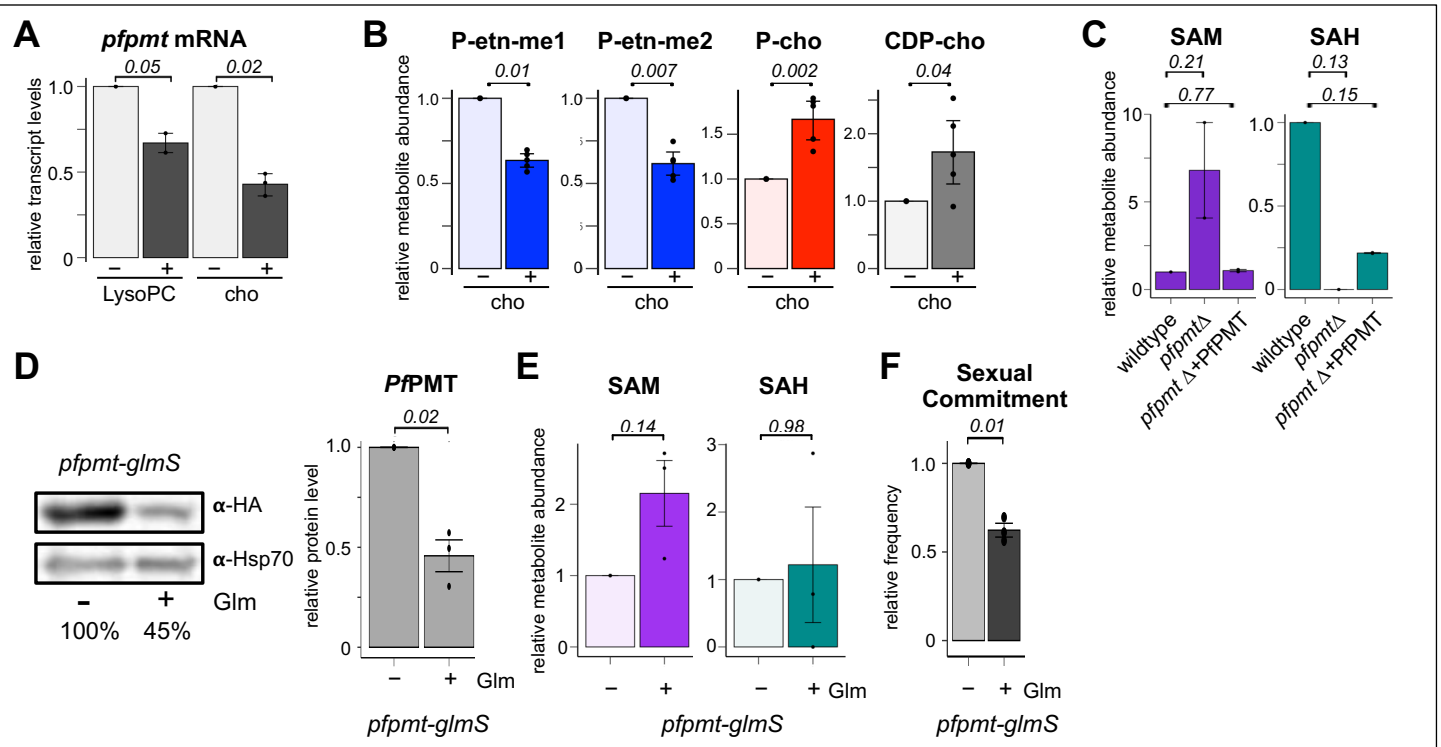

Figure 2. De novo synthesis of P-cho by *Pf*PMT is a major sink of SAM and source of SAH. (A) Down-regulation of *pfpmt* transcript abundance upon supplementation with P-cho precursors LysoPC and choline. Abundance was normalized to seryl-tRNA synthetase transcript and shown relative to no P-cho precursor supplementation. (n=2-3) **(B)** Choline supplementation results in increased P-cho due to choline scavenging but reduces *Pf*PMT activity as indicated by reduced levels of the mono- and di-methyl-phospho-ethanolamine intermediates. (n=4). **(C)** Loss of *Pf*PMT (*pfpmt*Δ) results in drastic changes in intracellular SAM and SAH levels that are restored after complementation (*pfpmt*Δ+*Pf*PMT). (n=2) **(D)** Inducible knockdown of *Pf*PMT upon addition of 2.5 mM glucosamine (Glm) in *Pf*PMT-glmS parasites significantly reduces *Pf*PMT protein abundance relative to *Pf*HSP70 loading control. (n=3) **(E-F)** Knockdown of *Pf*PMT increases intracellular SAM levels and reduces sexual commitment even in the absence of P-cho precursors (right panel) (n=3). Bar graphs indicates the mean values relative to the reference condition ± s.e.m. Italicized numbers are p-values from two-sided paired t-tests.

Intracellular SAM levels regulate sexual commitment.

To determine whether these changes in SAM and SAH abundance merely correlate with *Pf*PMT activity or directly regulate sexual commitment, we set out to manipulate their intracellular concentrations independently of *Pf*PMT activity and P-cho precursor abundance. We reasoned that if the availability of P-cho precursors suppresses sexual commitment by reducing *Pf*PMT's consumption of SAM, then this suppression should depend on overall SAM availability. In malaria parasites, SAM is generated solely by SAM synthetase (SAMS) from methionine. Malaria parasites are methionine auxotrophs and, unlike most eukaryotes, lack orthologs to enzymes able to regenerate methionine from homocysteine (Warrenfeltz et al., 2018), making parasite SAM synthesis fully dependent on methionine derived from host cell proteins or extracellular pools (Figure 3A). Removing extracellular methionine during a single commitment cycle substantially decreased intracellular methionine and SAM (Figure 3B) but had no discernable effect on parasite replication. In standard

growth medium containing 100 µM methionine, choline significantly suppressed commitment, but this suppressive effect was negated when methionine was removed from the growth media (Figure 3C).

Since methionine is critical for a variety of cellular functions including translation, we generated glucosamine-regulatable *pfsams-glmS* knockdown parasites to evaluate whether this effect was specific to SAM availability (Figure S4). Upon addition of glucosamine, protein levels of *Pf*SAMS were reduced by 58% (Figure 3D), which, even in the presence of choline, resulted in a two-fold reduction in SAM levels (Figure 3E) along with a more than 2.5-fold increase in sexual commitment (Figure 3F). Together, these findings demonstrate that sexual commitment is directly regulated by SAM availability.

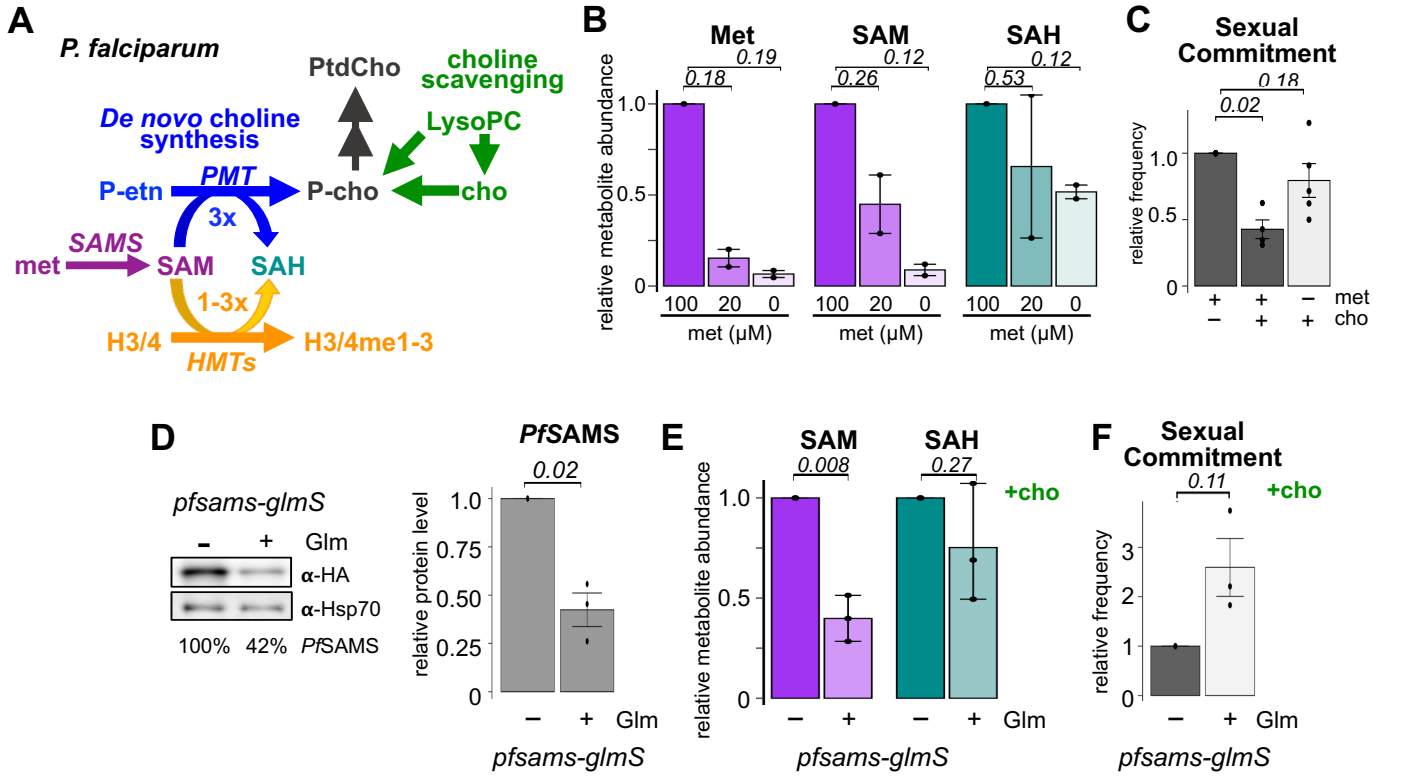

Figure 3. Intracellular SAM abundance regulates the frequency of sexual differentiation. (A) SAM and SAH are substrate and product, respectively, of both *de novo* P-cho synthesis and histone methylation. **(B)** Intracellular SAM abundance in growth medium containing standard (100 µM) or reduced levels of methionine (20 µM or 0 µM). (n=2) **(C)** Removal of extracellular methionine reverses the suppressive effects of choline supplementation (n=5). **(D-F)** Knockdown of *Pf*SAMS in *pfsams-HA-glmS* parasites by treatment with 2.5 mM glucosamine (Glm) **(D)**, reduced intracellular SAM by 59% **(E)**, and increased the sexual differentiation rate 2.5-fold **(F)** (n=3). Bar graphs indicates the mean values relative to the reference condition ± s.e.m. Italicized numbers are p-values from two-sided paired t-tests.

SAM, but not P-cho precursors, regulates sexual commitment in rodent malaria parasites.

Unlike in *P. falciparum*, supplementation with P-cho precursors had little to no effect on sexual commitment in the rodent malaria parasite *Plasmodium berghei* (Brancucci et al., 2017). In the context of our proposed model, where the consumption of SAM by *Pf*PMT provides the link between P-cho precursors and histone methylation, this observation is readily explained by the fact that the *pfpmt* ortholog was lost in the rodent

malaria parasite lineage, thereby decoupling P-cho availability from SAM and SAH abundance in rodent parasites (Figure 4A). However, since heterochromatin-mediated silencing of the *ap2-g* locus also controls sexual commitment in rodent parasites (Fraschka et al., 2018; Sinha et al., 2014), we hypothesized that commitment in *P. berghei* would never-the-less remain sensitive to changes in SAM availability. To test this, we generated SAMS knockdown parasites in *P. berghei* by creating a C-terminal fusion of the endogenous coding sequence with the ecDHFR-based destabilization domain (*pbsams-dd-ha*, Figure S5A-B). Upon removal of the stabilizing ligand trimethoprim, *Pb*SAMS expression was reduced by 60% in *pbsams-dd-ha* blood-stages (Figure 4B, Figure S5C) and resulted in a two-fold increase in sexual commitment (Figure 4C). This demonstrates that SAM availability regulates the rate of sexual commitment even when decoupled from PtdCho metabolism.

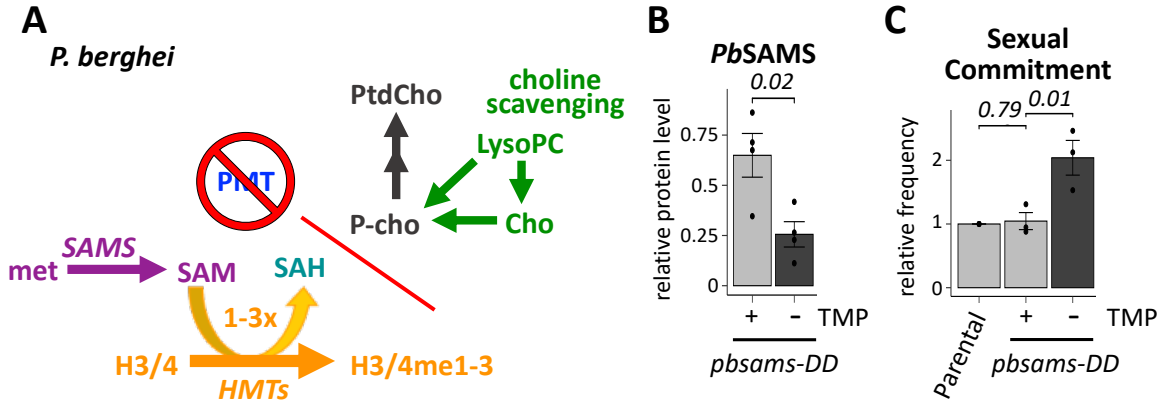

Figure 4. Intracellular SAM abundance also regulates commitment in Rodent Parasites. (A) Loss of PMT in rodent malaria parasites, such as *P. berghei,* decouples SAM and SAH from PtdCho synthesis. **(B)** Removal of the stabilizing ligand TMP from *P. berghei pbsams-DD* knockdown parasites reduced *Pb*SAMS by 61% and **(C)** resulted in a 2-fold increase in sexual differentiation (n=3-4)**.** Bar graphs indicates the mean values relative to the reference condition ± s.e.m. Italicized numbers are p-values based on two-sided paired t-tests.

Both SAM and SAH regulate heterochromatin maintenance at the *pfap2-g* locus.

In higher eukaryotes, histone methylation dynamics and gene regulation have been shown to be responsive to changes in SAM and SAH metabolism (Li et al., 2015; Mentch et al., 2015; Shyh-Chang et al., 2013; Ye et al., 2017; 2019). Methionine depletion and reduction in SAM abundance led to decreased methylation of specific histone modifications including H3K4me3, H3K9me3, H3K4me2, and H3K36me3, with H3K4me3 exhibiting the most profound changes and leading to a change in gene expression (Mentch et al., 2015; Sutter et al., 2013; Ye et al., 2017). Since changes in intracellular SAM directly alter commitment rates (Figure 3), we tested whether these changes could substantially alter the abundance or distribution of the main histone methylation marks associated with silencing (H3K9me3) and activation (H3K4me3) of *pfap2-g* (Figure 5) (Karmodiya et al., 2015; Salcedo-Amaya et al., 2009). To evaluate the effect of SAM on histone methylation

patterns we compared the distribution of these marks in the presence of abundant extracellular choline and methionine when SAM levels are high to conditions when the absence of these metabolites in the growth medium results in low SAM levels (Figure 5A), and elevated rates of sexual commitment (Figure 5B).

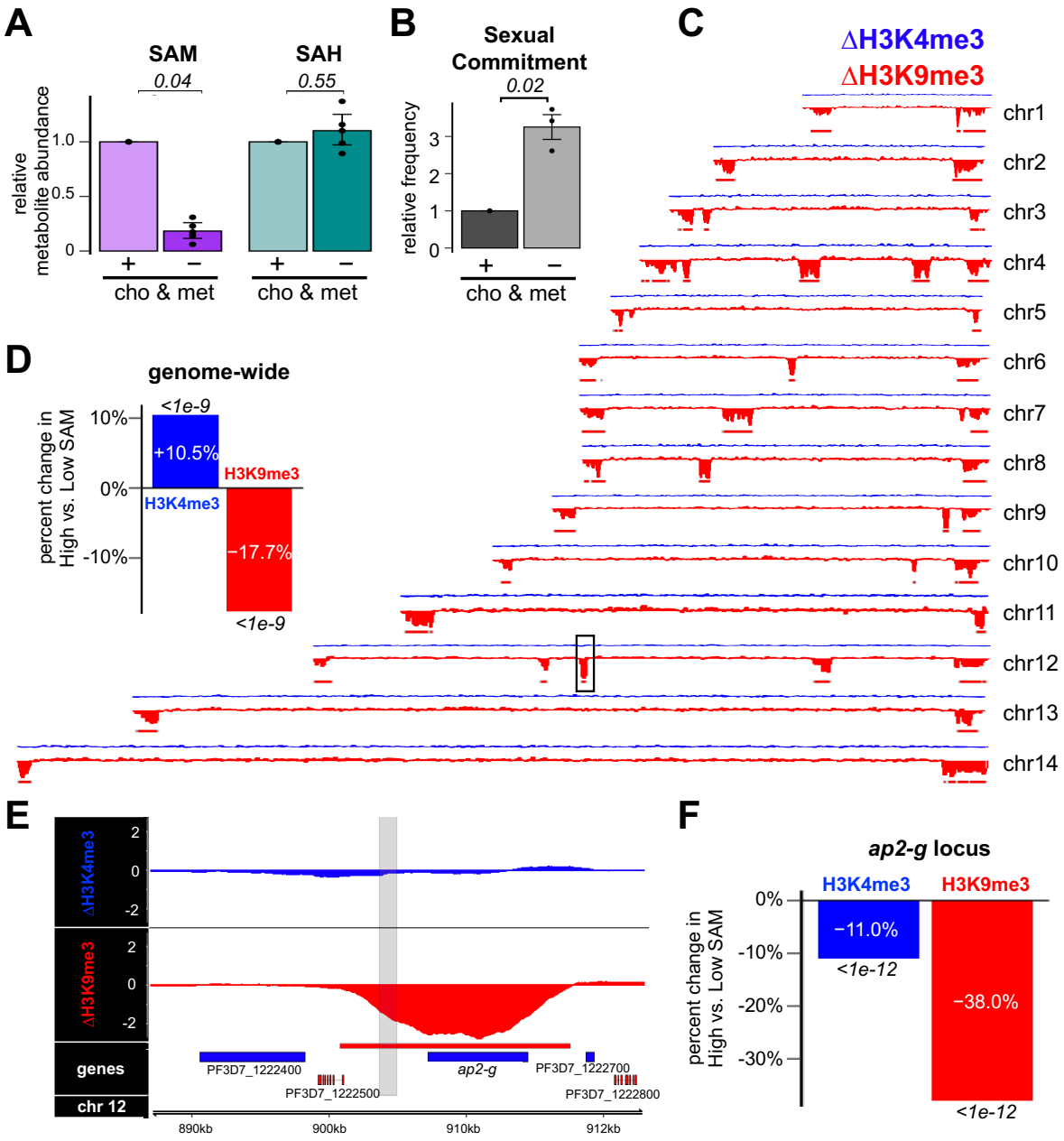

Figure 5. Changes in intracellular SAM alter the efficiency of heterochromatin maintenance at the *pfap2-g* locus. **(A-B)** Relative intracellular abundances of SAM and SAH **(A)**, and sexual commitment **(B)** under high SAM vs. low SAM conditions (n=3-4). **(C)** Differences in the distribution of H3K4me3 (blue) and H3K9me3 (red) between parasites grown in low SAM (–cho, –met) versus high SAM (+cho, +met) conditions as determined by CUT& RUN. The box on chromosome 12 indicates location of the *pfap2-g* locus. Red bars indicate regions of heterochromatin under high SAM conditions (n=2). **(D)** Mean genome-wide change in H3K4me3 (blue) and H3K9me3 (red) coverage in low SAM versus high SAM conditions. **(E)** Changes in the distribution of H3K4me3 (blue) and H3K9me3 (red) at the *pfap2-g* locus under conditions between parasites grown in low SAM (–cho, –met) versus high SAM (+cho, +met) conditions. **(F)** Mean change in coverage across the *pfap2-g* heterochromatin peak (red bar) of H3K4me3 (blue) and H3K9me3 (red) between parasites grown in low SAM versus high SAM conditions.

In contrast to H3K4me3, which was somewhat elevated when intracellular SAM was low, we observed genome-wide reductions in the abundance of the repressive H3K9me3 mark (Figure 5C-D) under low SAM conditions when compared to high SAM conditions. This reduction in H3K9me3 was observed in regions of sub-telomeric heterochromatin as well as for non-subtelomeric heterochromatin islands (Figure 5C).

Closer examination of the *pfap2-g* locus on chromosome 12 found that H3K9me3 occupancy across the locus was reduced by 38.0% under low SAM conditions (Figure 5E-F). At the leading edge of the heterochromatin island, which overlaps the promoter region containing the *Pf*AP2-G binding sites that drive the transcriptional feedback loop, this reduction was even more profound (-42.0% under low SAM, $p < 1e\text{-}12$). These data demonstrate that H3K9me3 occupancy at the *pfap2-g* locus is responsive to changes in SAM. Under conditions of choline and methionine depletion, cellular pools of SAM are reduced which impair the maintenance of H3K9me3 placement at the *pfap2-g* locus as the parasite replicates its genome 20-30x times during schizogony.

Each transfer of a methyl group from SAM generates one equivalent of SAH, which can act as a potent feedback inhibitor for many SAM-dependent methyltransferases (Reguera et al., 2007). De novo P-cho synthesis by *Pf*PMT therefore represents not only a major sink of SAM but also an equivalently large source of intracellular SAH (Figure 2, Figure S1). To test if direct changes to the intracellular levels of SAH alter sexual commitment, we treated parasites during the commitment cycle with 3-deaza-adenosine (3-DZA), a potent inhibitor of SAH hydrolase (SAHH), the enzyme that converts SAH into adenine and homocysteine (Figure 6A) (Bujnicki et al., 2003; Chiang, 1998). Treatment with 3-DZA in the presence of abundant methionine and choline increased both SAH and SAM levels, the latter likely due to reduced consumption of SAM by methyltransferases as the result of feedback inhibition by the increasing SAH levels (Figure 6B), and more than doubled sexual commitment, fully reversing the suppressive effects of choline supplementation (Figure 6C). These results demonstrate that elevating SAH levels is sufficient to increase sexual commitment rates, even when SAM is highly abundant. These data are in alignment with a previous study which found that homocysteine, the metabolic product and feedback inhibitor of SAHH which accumulates in culture and in the serum of infected patients, induces gametocytogenesis in culture (Beri et al., 2017).

Histone methyltransferases differ in their susceptibility to feedback inhibition by SAH (Luo, 2018). Since suppression of commitment with choline reduced intracellular SAH levels but left SAM levels largely unchanged, we wanted to also evaluate whether high SAH was sufficient to impair heterochromatin maintenance even when SAM is abundantly available. While elevating SAH reduced genome-wide H3K4me3 abundance by 8.3%, it had even more profound effects on the H3K9me3 silencing mark, which was reduced 22.3% genome-wide (Figure 6D-E). H3K9me3 occupancy across the *pfap2-g* locus on chromosome 12 was

reduced by 29.3% under high SAH conditions (Figure 6F-G). At the region of the locus containing the *Pf*AP2-G binding sites that drive the transcriptional feedback loop, this reduction was more profound at -39.2% under high SAH, $p < 1e^{-12}$. Thus, H3K9me3 occupancy at the *pfap2-g* locus is responsive to changes in SAH as well as SAM. Even when SAM is abundant, increasing the levels of SAH also impairs heterochromatin maintenance at the *pfap2-g* locus, increasing sexual commitment (Figure 6).

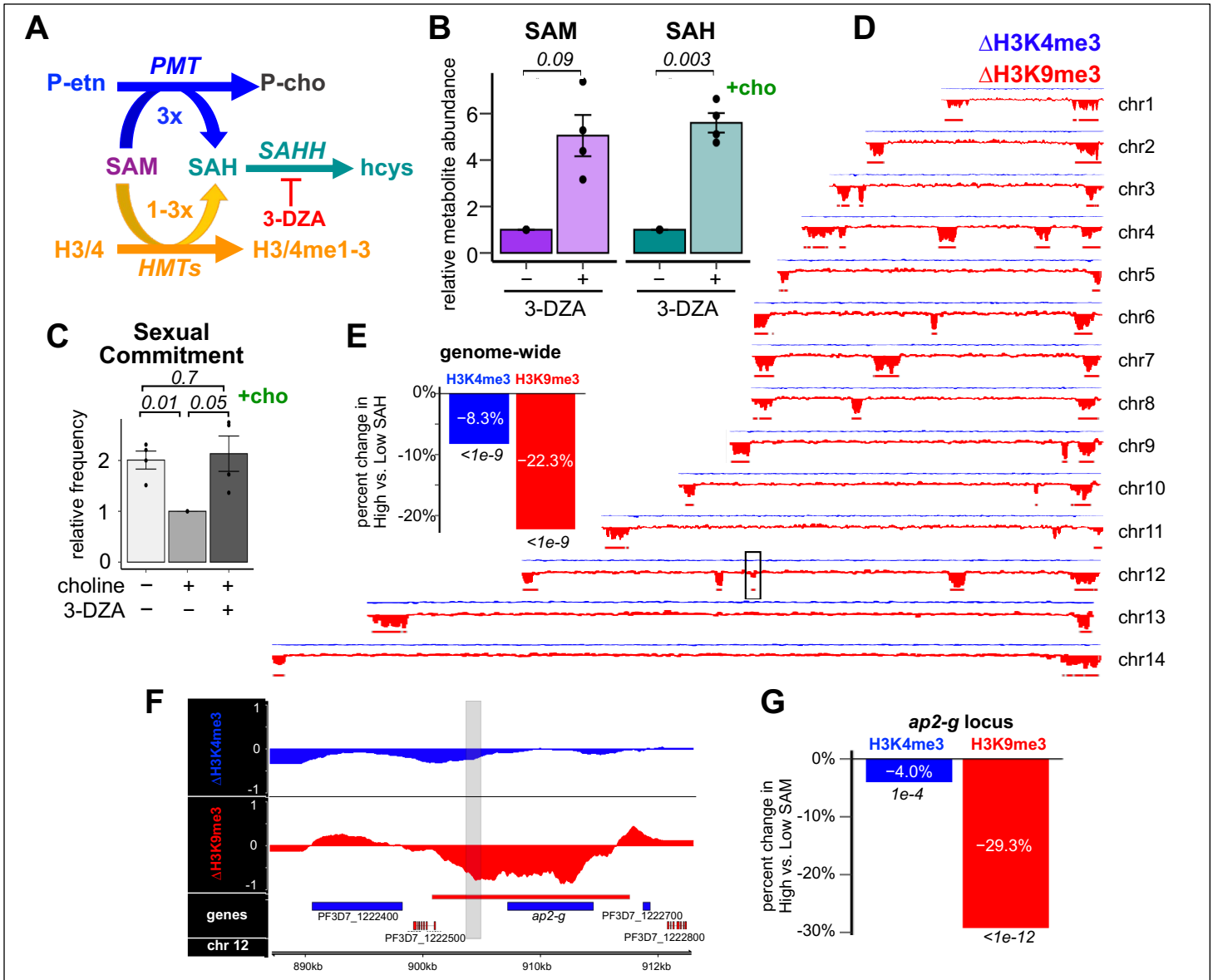

Figure 6. Changes in intracellular SAH alter the efficiency of heterochromatin maintenance at the *pfap2-g* locus. **(A-C)** Inhibition of SAHH with 3-DZA increases intracellular SAM and SAH (B), as well as sexual commitment **(C)** (n=3-4). **(D)** Genome-wide differences in the distribution of H3K4me3 (blue) and H3K9me3 (red) between parasites grown in high SAH (+cho, +met, +3-DZA) versus low SAH (+cho, +met) condition as determined by CUT& RUN. The box on chromosome 12 indicates location of the *pfap2-g* locus. Red bars indicate regions of heterochromatin. **(E)** Mean genome-wide change in H3K4me3 (blue) and H3K9me3 (red) coverage in high SAH versus low SAH conditions. **(F)** Differences in the distribution of H3K4me3 (blue) and H3K9me3 (red) between parasites grown in high SAH versus low SAH conditions at the *pfap2-g* locus on chromosome 12. **(G)** Mean change in coverage across the *pfap2-g* heterochromatin peak (red bar) of H3K4me3 (blue) and H3K9me3 (red) between parasites grown in high SAH versus low SAH conditions. Italicized numbers are p-values based on two-sided paired t-tests for metabolite abundance or based on HOMER annotatePeaks and DESeq2 for histone modification abundance.

DISCUSSION

Malaria parasites have evolved sophisticated mechanisms to sense and adapt to the diverse physiological niches they occupy during their life cycle. The switch from asexually replicating blood stage parasites to male and female gametocytes requires balancing a trade-off between maintaining in-host persistence and maximizing transmission between hosts. Several metabolites have been implicated in affecting this switch. Serine and homocysteine both increase frequencies of sexual differentiation (Beri et al., 2017; Gulati et al., 2015), while LysoPC and its metabolic product, choline, both act as potent suppressors of sexual commitment (Brancucci et al., 2017). Additionally, the concentrations of these precursors are especially low in the bone marrow, the primary site of *P. falciparum* gametocytogenesis (Brancucci et al., 2017; Joice et al., 2014). Maturation in the bone marrow protects immature gametocytes from splenic clearance until they mature into highly deformable stage V gametocytes that are able to pass through the spleen (Neveu et al., 2020b; Tibúrcio et al., 2012). However, the molecular mechanisms that allow the parasite to modulate its frequency of sexual differentiation in response to these metabolites remained unknown.

Here we show that a drop in P-cho precursors leads to a decrease in intracellular SAM and rise in SAH as the result of increased *de novo* P-cho synthesis by PMT. These changes in SAM and SAH reduce the efficiency of H3K9me3 maintenance as the parasite replicates its genome 20-30 times during schizogony. This includes the single-gene heterochromatin island on chromosome 12 that is responsible for silencing the expression of the transcription factor *Pf*AP2-G during asexual replication. Due to the ability of *Pf*AP2-G to drive its own expression, inefficient silencing increases the frequency at which leaky transcription exceeds the expression level that triggers this feedback loop and commits parasites to sexual differentiation (Figure 7).

Intriguingly, in malaria parasites methylation of H3K9 is more sensitive to changes in SAM and SAH than H3K4 methylation, unlike what has been reported for higher eukaryotes. This suggests future examination of whether the Km and Ki for SAM and SAH of *Pf*SET3, the parasite's only Su(var)3-9 methyltransferase, are in the range of the intracellular concentrations of these two metabolites, allowing their concentration to directly regulate the deposition of the H3K9me3 silencing mark.

Our model also explains the previously described observation that in rodent parasites sexual commitment is not responsive to P-cho precursors, as the loss of PMT in the rodent malaria parasite lineage decouples PtdCho synthesis from SAM, SAH, and histone methylation. Strikingly, this loss of PMT in rodent malaria parasites was accompanied by a lineage-specific expansion of the *fam-a* gene family from a single copy in the primate lineage to 42-215 copies (Otto et al., 2014). Members of this family contain the steroidogenic acute regulatory-related lipid transfer (START) domain and which have been show to transport

PtdCho (Fougère et al., 2016). Without the ability generate this key phospholipid *de novo*, this expansion presumably allows rodent malaria parasites to scavenge a full complement of PtdCho precursors.

In summary, changing availability of host LysoPC results in a shift in intracellular SAM/SAH which leads to changes in histone methylation, in particular the H3K9me3 silencing mark. Inefficient silencing at the *pfap2-g* locus increases the frequency of activating the transcriptional feedback loop that commits parasites to sexual differentiation in *P. falciparum.* This allows parasites to increase sexual differentiation in the bone marrow where LysoPC is low and where gametocytes can develop without the risk of splenic clearance.

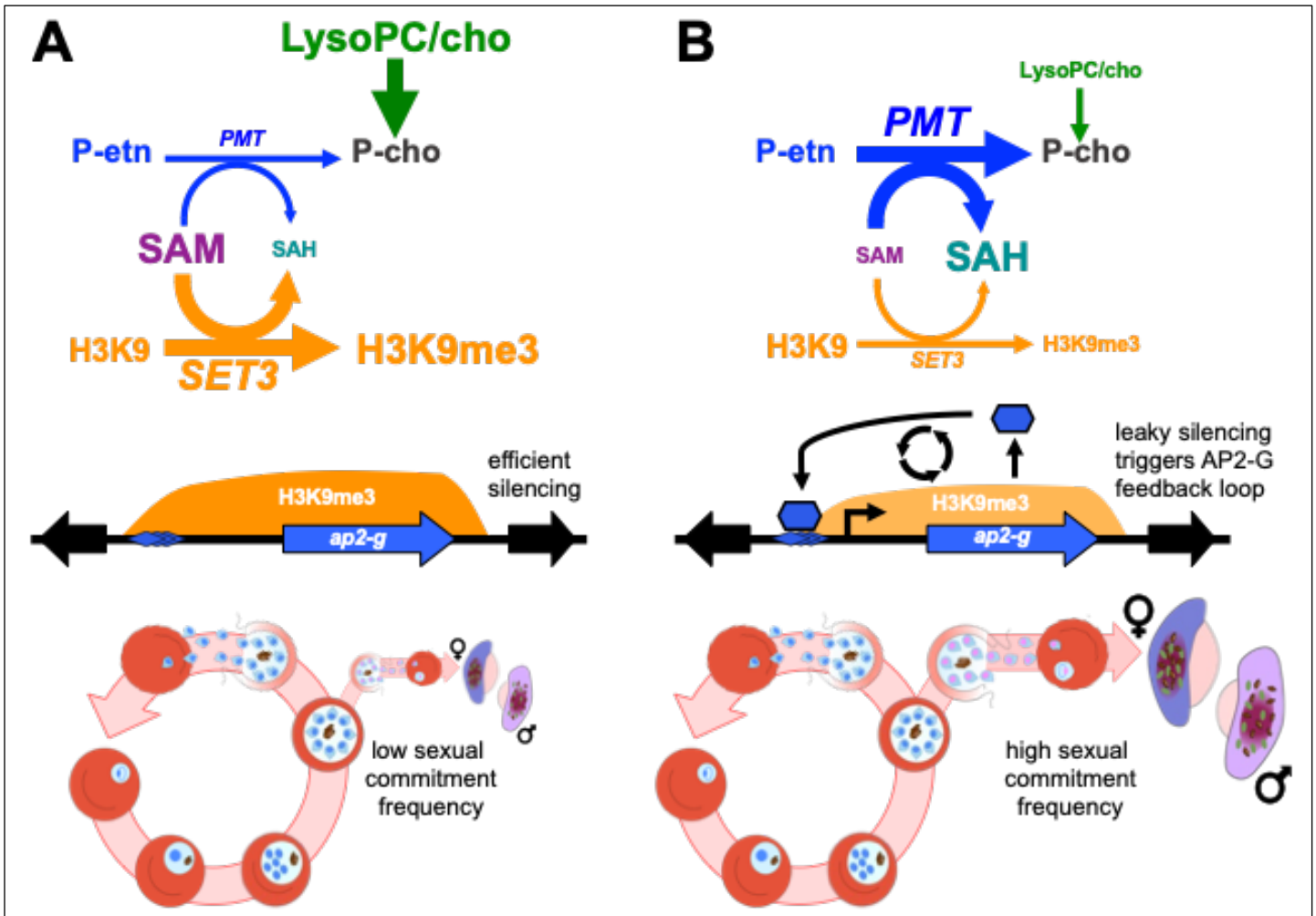

Figure 7. Metabolic competition between PMT and H3K9 methylation controls the rate of sexual commitment.
(A) When P-cho precursors are available, H3K9me3 heterochromatin is efficiently maintained during schizogony resulting in low sexual commitment. **(B)** When P-cho precursors are scarce, increased *de novo P*-cho synthesis by *Pf*PMT reduces SAM and increases SAH, both of which impair deposition H3K9me3 genome. Leaky silencing at the *pfap2-g* locus increases the probability of activating the positive transcriptional feedback loop, thereby increasing the frequency of commitment to sexual differentiation.

ACKNOWLEDGMENTS

General: We wish to thank Dr. Choukri Ben Mamoun (Yale School of Medicine) for the gift of the *pfpmt* knockout and complemented lines and the Weill Cornell Medicine genomics core for technical support.

Funding: This work was supported by funds from Weill Cornell Medicine (BK), NIH 1R01 AI141965 (BK), NIH 1R01 AI138499 (KWD), NIH 5F31AI136405-03 (CH), NIH R25 AI140472 (KYR), the Fundação para a Ciência e Tecnologia (MMM, DRIVER-LISBOA-01-0145-FEDER-030751) and "laCaixa" Foundation (MMM, under the agreement HR17/52150010).

Author contributions: Conceptualization: BFCK, KWD, MMM; Methodology: BFCK, CTH, MMM; Investigation: CTH, XT, LNV, IMM; Software, Formal Analysis, Data Curation: BFCK, CTH, XT; Writing – Original Draft: CTH Writing – Review & Editing: BFCK, CTH, MMM; Visualization: BFCK, CTH; Supervision: BFCK, KYR, MMM; Project Administration: B.F.C.K; Funding Acquisition: BFCK, KWD, MMM

Competing interests: The authors declare no competing interests.

Data and materials availability:

All data needed to evaluate the conclusions in the paper are present in the paper or the supplementary materials. Raw and processed CUT & RUN data can be obtained from the NCBI Gene Expression Omnibus (GSE197916). The CUT & RUN analysis pipeline is available at https://github.com/KafsackLab/MetChoH3K9me3.

MATERIALS AND METHODS

P. falciparum cell culture

The parasite strains used for this study were NF54 obtained from BEI Resources and the *Pf-peg4*-tdTomato (McLean et al., 2019). Cultures were maintained using established culturing techniques (Moll et al., 2008). Standard complete media was RPMI-1640 supplemented with 25 mM HEPES, 368 µM hypoxanthine, 1 mM sodium hydroxide, 24 mM sodium bicarbonate, 21 µM gentamycin (Millipore Sigma), with Albumax II Lipid-Rich BSA (Gibco), unless otherwise stated. Concentrations for choline and LysoPC supplementation were used according to (Brancucci et al., 2017). See Supplementary Table 1 for changes to media compositions used throughout this manuscript. RBCs or cultures were washed three times with respective experimental media conditions at the start of each change in media condition.

Generation of *Pf*SAMS-glmS and *Pf*PMT-glmS conditional knockdown lines

The 3' portion of the coding sequence for *pfsams* (577-1206bp) and *pfpmt* (651-1217bp) was amplified from gDNA and cloned by Gibson assembly into the pSLI-HAx3-glmS plasmid (gift from Professor R. Dzikowski) (Prommana et al., 2013) following NotI and XmaI double digest. Following transfection of NF54 parasites, cultures were selected for the presence of the plasmid with 4nM WR99210 (gift of Jacobus Pharmaceuticals), follow by selection for integrants with G418 (Millipore Sigma). Single-crossover integration of the plasmid was confirmed via PCR (Figures S3 and S5), and parasites were cloned to isolate a population with single cross-over lacking any remaining WT loci. Integrated parasite lines were maintained under G418 drug pressure.

Animal Maintenance

Animal research was conducted at the Instituto de Medicina Molecular (Lisboa, Portugal). All protocols were approved by the animal ethics committee (ORBEA committee) at the institute and performed according to national and European regulations. BALB/c mice (age 5-8 weeks; males) were purchased from Charles River Laboratories (Saint-Germain-sur-l'Arbresle, France), kept in specific-pathogen-free conditions, and subjected to regular pathogen monitoring by sentinel screening. Experimental animals were randomly assigned and allowed free access to water and food.

Generation of *Pb*SAMS-DD conditional knockdown parasites

Wild-type *P. berghei* ANKA strain was obtained from the MR4 repository (Manassas, Virginia). *P. berghei pbsams-DD* parasite line was obtained by double crossover homologous recombination. To do so, parasites were transfected by electroporation of purified schizonts, harvested on day 7-10 post transfection and

genotyped by PCR. Transgenic parasites were then dilution cloned and further stored at -80 °C in frozen blood vials, containing 10^7 blood stage parasites.

Recombinant parasites carrying the human dihydrofolate reductase (*hdhfr*) gene cassette were positively selected by treatment of mice with pyrimethamine and trimethoprim to stabilize *Pb*SAMS. Confirmation of transgenic parasite genotype, construct integration at the desired genomic loci and elimination of WT locus were assessed by PCR. Blood from the tail vein of infected mice was collected in 200µL of 1x PBS and genomic DNA was isolated using the NZY Blood gDNA Isolation Kit (NZYTech), according to manufacturer's guidelines. Stabilization of *Pb*SAMS-DD fusion protein throughout infection was achieved in vivo, by administration of trimethoprim (TMP) to mice (0.25 mg/ml of TMP in drinking water), 2 days prior to infection.

Quantification of *Pb*SAMS knockdown

All steps of parasite pellet extraction protocol were performed at 4ºC to minimize protein degradation and all centrifugations were executed at 1000 x g for 10 min. Mice were sacrificed at day 4 post infection, 1mL of blood was collected by cardiac punction, washed in 10mL of 1x PBS and centrifuged. Packed erythrocytes were saponin-lysed in 0.15% saponin and centrifuged. Parasite pellet was washed twice in PBS containing 1x Proteinase inhibitor cocktail (Roche cOmplete Protease inhibitor tablets, EDTA free). Parasite pellet was then resuspended in lysis buffer (4 % SDS; 0.5 % Triton X-114 in 1x PBS), incubated on ice for 10 min, centrifuged at 21000 x g for 10 min and the supernatant was collected. Total protein content was determined using the Bio-Rad protein assay kit according to manufacturer's instructions. Protein samples diluted in 5x SDS sample buffer (NZYTech) were denatured at 95º for 10 min and resolved in an 8% polyacrylamide gel (SDS-PAGE). Proteins were blotted into a nitrocellulose membrane by wet transfer at 200mA for 2 hours. Primary antibodies, mouse anti-HA antibody (1:1000, from Covance) and rabbit anti-Bip (1:2000, GeneScript) were incubated overnight at 4ºC. Secondary antibodies, anti-mouse horseradish peroxidase (HRP)-conjugated and anti-rabbit HRP (1:10000, Jackson ImmunoResearch Laboratories) were incubated at RT for 1 hour. Signal detection was obtained using Luminata Crescendo Western HRP substrate (Merck Milipore®) and the ChemiDoc XRS+ Gel Imaging System (BioRad). Protein band quantification was performed on Image Lab software (version 5.0) using BIP levels for normalization.

Quantification of gametocytes in *Pb*SAMS-DD-HA parasites

Mice infections were performed by intraperitoneal inoculation of 1×10^6 infected red blood cells (iRBCs) obtained by passage in the correspondent BALB/c background mice. Parasitemia (% of iRBCs) was monitored

daily and gametocytemia (% of mature gametocytes) was determined on day 3 after infection, by microscopic analysis of Giemsa-stained blood smears. A total of 5-10 thousand RBCs were analysed in randomly acquired images and semi-automatically quantified using Image J software (http://rsbweb.nih.gov/ij).

Induction and quantification of *P. falciparum* sexual commitment

Synchronous gametocyte induction was performed as previously described (Poran et al., 2017). Briefly, parasites were double-synchronized with 5% sorbitol to achieve a synchrony of ± 6h in the previous cycle. Synchronized ring-stage parasites were set up at 1.5% parasitemia (1% hematocrit) in 96-well, flat bottom plates under specific nutrient conditions to induce sexual commitment. Following reinvasion, on the first day of gametocyte development (D+1), ring-stage parasitemia was determined using flow cytometry and 50mM *N*-acetyl-D-glucosamine was added for 5 consecutive days. Gametocytes were then counted on day 6 (D+6) and commitment rate was determined by dividing the D+6 gametocytemia by the D+1 parasitemia assessed prior to *N*-acetyl-D-glucosamine addition. Gametocytes induced using the Pf-*peg4*-tdTomato fluorescent gametocyte reporter line were counted using flow cytometry(McLean et al., 2019).

Metabolite Analysis

Synchronous *P. falciparum* parasites were grown from 8hpi to 34hpi ± 6 hpi (100mL, 3% hematocrit, 5-6% parasitemia) under the indicated growth conditions. Infected red blood cells (iRBC) were then purified to > 90% purity using a 70/40% percoll/sorbitol density gradient and centrifugation (4700 G for 15 minutes at room temperature), then washed three times with minimal RPMI. Following isolation, equal numbers of isolated iRBC, as determined by the Beckman Coulter Z1 Coulter Particle Counter, were then re-incubated in their respective treatment conditions for four more hours to allow parasites to recover from percoll/sorbitol isolation. Following recovery, the purity of iRBCs was assessed using flow cytometry, cells were then pelleted, washed once with 1 mL of 1x PBS, and quickly lysed with 500 µL of 90% ultrapure HPLC Grade methanol (VWR), followed by exactly 10 seconds of vortexing before being stored in dry ice. Lysed samples were then centrifuged at top speed at 4°C and supernatant collected for metabolite analysis. Uninfected red blood cells (uRBC) were incubated under the same treatment conditions as iRBC, counted, and methanol extracted to distinguish iRBC metabolite signal from uRBC signal. Extracted metabolites were stored at -80°C. LC-MS based metabolomic analysis was performed as previously described (Ballinger et al., 2019). 10 µL of extract was separated on an Agilent 1290 Infinity LC system containing a Cogent Diamond Hydride Type C silica column (150 mm × 2.1 mm; Microsolv Technologies). Acquisition was performed on an Agilent 6230 TOF mass spectrometer (Agilent Technologies, Santa Clara, CA) employing an Agilent Jet Stream electrospray ionization

source (Agilent Technologies, Santa Clara, CA) operated in high resolution, positive mode. Metabolite identification was verified by exact mass (to 35 ppm) and co-elution with authentic standards purchased from Millipore Sigma. Batch feature extraction and chromatographic alignment across multiple data files was performed using the Agilent MassHunter Profinder software and extracted metabolite data was exported for further statistical analysis using R.

Western Blotting

*Pf*PMT-glmS and *Pf*SAMS-glmS knockdown western blots were performed using whole cell lysate. Ring-stage parasites (12hpi ± 6 hpi) were treated with or without 2.5mM glucosamine (VWR) to induce protein knockdown as previously described. Parasites were saponin lysed at 36hpi ± 6 hpi and whole cell extract collected in SDS sample buffer, then boiled for 10 minutes. Proteins were then separated on 12% SDS PAGE and transferred to a PVDF membrane (Millipore Sigma, 0.2 µM). Membranes blocked with 5% milk were then probed with anti-HA (1:2000, Abcam, ab9110), and anti-hsp70 (1:2000, StressMarq SPtdCho-186) primary antibody solutions, followed by anti-rabbit IgG (1:5000, Millipore Sigma 12-348) secondary. Chemiluminescence was measured using the Azure c-Series imaging systems (Azure Biosystems) and quantified using the Fiji open-source image processing package based on ImageJ.

Quantification of changes in H3K9me3 and H3K4me3 abundance and distribution.

H3K9me3 and H3K4me3 abundances were measured by Cleavage Under Targets & Release Using Nuclease (CUT & RUN) (Skene et al., 2018) adapted for *P. falciparum*. Approximately 1 x 10^7 percoll/sorbitol isolated schizonts (34-38 hpi) per sample were washed three times with 1 ml wash buffer (20 mM HEPES at pH 7.5, 150 mM NaCl, 0.5 mM Spermidine, and 1 × Roche complete protease inhibitor) at room temperature and resuspended in 225ul of wash buffer. 25ul of Concanavalin A-coated beads were washed and resuspended in binding buffer (20 mM HEPES–KOH at pH 7.5, 10 mM KCl, 1 mM CaCl2, 1 mM MnCl2) before being added to each sample. Samples were then rotated for 10 minutes at room temperature. Then, samples were placed on a magnetic stand to clear (30s to 2 minutes) and remove all the liquid. Samples were washed 3x's with DIG wash buffer (wash buffer with 0.025% digitonin). For each sample, 150µl of antibody wash buffer was added (wash buffer, 0.025% digitonin, and 2 mM EDTA at pH 8.0) with H3K4me3 (0.005µg/µl, C15410003-50, Diagenode), H3K9me3 (0.005µg/µl, ab8898, abcam), or IgG isotype control (0.005µg/µl, 02-6102, ThermoFisher) was added to the sample tube and incubated at 4 °C, rotating, overnight. Following antibody incubation, samples were placed on a magnetic stand to clear and pull off the liquid, then washed 3 x's with DIG wash buffer, 150 µl of ProteinA/G-MNASE fusion protein (dilution 1:60, 15-1016, EpiCypher) in DIG wash

buffer and rotated at 4 °C for 1 hour. After washing samples 3x's with DIG wash buffer, samples were then washed 3x's with Low Salt Rinse Buffer (20 mM HEPES–NaOH at pH 7.5, 0.025% digitonin, 0.5 mM spermidine). 200 µl of ice-cold incubation buffer (3.5 mM HEPES–NaOH at pH 7.5, 100mM $CaCl_2$, 0.025% DIG) was added and samples were equilibrated at 0 °C for 30 minutes to achieve targeted digestion. Digestion was then stopped by adding 200 µl of stop buffer (170 mM NaCl, 20 mM EGTA at pH 8.0, 20 mM EGTA, 0.0.25% digitonin, 25 µg/mL glycogen, 50 µg/mL RNase A). After incubation at 37 °C for 30 minutes to release soluble fragments, samples were digested by adding 2.5 µL proteinase K (20 mg/ml) and 2 µL 10% SDS, and then incubated at 50 °C for 1 hour. DNA fragments were purified with phenol–chloroform–isoamyl alcohol and washed by ethanol precipitation, and finally dissolved in 30 µL TE buffer (1mM Tris-HCl pH 8, 0.1 mM EDTA).

Library construction was carried out using NEBNext Ultra II DNA Library Prep Kit for Illumina (E7645S, NEB). 4ng of fragmented DNA was used for end-repair/A-tailing, ligation, and post ligation cleanup with 1.7x volumes of AMPure XP beads (Catalog number, company). Following cleanup, PCR amplification was performed using 2x KAPA HotStart ready mix (Catalog number, company) and NETFLEX primer mix (Catalog number, Bio Scientific) with PCR program: 1 min @ 98° C/15 cycles: 10 sec @ 98° C/1 min @ 65° C// 5min @ 65° C// hold 4° C. PCR products were size selected with 0.8x volumes, then 1.2x volumes of AMPure XP beads. Beads were then washed twice with 80% ethanol and DNA eluted with 0.1x TE and used for sequencing in a Nextseq2000 system as paired-end reads, following quality control.

After sequencing, raw reads were trimmed using Trimmomatic v0.38 (Bolger et al., 2014) to remove residual adapter sequences and low quality leading and trailing bases. Both paired and unpaired reads were retained for read lengths that were at least 30 bases after trimming. Trimmed paired reads were aligned to the PlasmoDB version 46 *P. falciparum* 3D7 reference genome (Warrenfeltz et al., 2018) using BWA v.0.7.1 (Li and Durbin, 2009). SAMtools v.1.10 (Li et al., 2009) was used to remove low quality alignments as well as sort and index sample files. Normalized fold enrichment tracks were generated by using the MACS2 v.2.2.7.1 (Zhang et al., 2008) callpeak function with settings: -f BAMPE -B -g 2.3e7 -q 0.05 –nomodel –broad –keep-dup auto –max gap 500. Bedgraph outputs were then passed into the bdgcmp function with the setting -m FE (fold enrichment) to generate signal tracks to profile histone modification enrichment levels compared to whole genome. Peak sets from replicates were compared with Bedtools intersect v2.26.0 (Quinlan and Hall, 2010), and peaks that overlapped by at least 1 bp were considered shared. Fold enrichment bedgraphs and peak sets were then output to RStudio Server (v1.4.1717) for further analysis using the GenomicRanges Package v.1.44.0 (Lawrence et al., 2013) and visualized with the GViz v1.38.1 package (Hahne and Ivanek, 2016) within the Bioconductor project (release 3.13) (Huber et al., 2015). The full analysis pipeline can be found at https://github.com/KafsackLab/MetChoH3K9me3.

REFERENCES

Ballinger, E., Mosior, J., Hartman, T., Burns-Huang, K., Gold, B., Morris, R., Goullieux, L., Blanc, I., Vaubourgeix, J., Lagrange, S., et al. (2019). Opposing reactions in coenzyme A metabolism sensitize Mycobacterium tuberculosis to enzyme inhibition. Science *363*.

Beri, D., Balan, B., Chaubey, S., Subramaniam, S., Surendra, B., and Tatu, U. (2017). A disrupted transsulphuration pathway results in accumulation of redox metabolites and induction of gametocytogenesis in malaria. Sci. Rep. *7*, 40213.

Bobenchik, A.M., Witola, W.H., Augagneur, Y., Lochlainn, L.N., Garg, A., Pachikara, N., Choi, J.-Y., Zhao, Y.O., Usmani-Brown, S., Lee, A., et al. (2013). Plasmodium falciparum phosphoethanolamine methyltransferase is essential for malaria transmission. Proc Natl Acad Sci USA *110*, 18262–18267.

Bolger, A.M., Lohse, M., and Usadel, B. (2014). Trimmomatic: a flexible trimmer for Illumina sequence data. Bioinformatics *30*, 2114–2120.

Brancucci, N.M.B., Bertschi, N.L., Zhu, L., Niederwieser, I., Chin, W.H., Wampfler, R., Freymond, C., Rottmann, M., Felger, I., Bozdech, Z., et al. (2014a). Heterochromatin protein 1 secures survival and transmission of malaria parasites. Cell Host Microbe *16*, 165–176.

Brancucci, N.M.B., Gerdt, J.P., Wang, C., De Niz, M., Philip, N., Adapa, S.R., Zhang, M., Hitz, E., Niederwieser, I., Boltryk, S.D., et al. (2017). Lysophosphatidylcholine Regulates Sexual Stage Differentiation in the Human Malaria Parasite Plasmodium falciparum. Cell *171*, 1532–1544.e15.

Brancucci, N.M.B., Witmer, K., Schmid, C., and Voss, T.S. (2014b). A var gene upstream element controls protein synthesis at the level of translation initiation in Plasmodium falciparum. PLoS ONE *9*, e100183.

Bujnicki, J.M., Prigge, S.T., Caridha, D., and Chiang, P.K. (2003). Structure, evolution, and inhibitor interaction of S-adenosyl-L-homocysteine hydrolase from Plasmodium falciparum. Proteins: Structure, Function, and Bioinformatics *52*, 624–632.

Chiang, P.K. (1998). Biological effects of inhibitors of S-adenosylhomocysteine hydrolase. Pharmacol Ther *77*, 115–134.

Coleman, B.I., Skillman, K.M., Jiang, R.H.Y., Childs, L.M., Altenhofen, L.M., Ganter, M., Leung, Y., Goldowitz, I., Kafsack, B.F.C., Marti, M., et al. (2014). A Plasmodium falciparum Histone Deacetylase Regulates Antigenic Variation and Gametocyte Conversion. Cell Host Microbe *16*, 177–186.

Drakeley, C., Sutherland, C., Bousema, J.T., Sauerwein, R.W., and Targett, G.A.T. (2006). The epidemiology of Plasmodium falciparum gametocytes: weapons of mass dispersion. Trends in Parasitology *22*, 424–430.

Filarsky, M., Fraschka, S.A., Niederwieser, I., Brancucci, N.M.B., Carrington, E., Carrió, E., Moes, S., Jenoe, P., Bartfai, R., and Voss, T.S. (2018). GDV1 induces sexual commitment of malaria parasites by antagonizing HP1-dependent gene silencing. Science *359*, 1259–1263.

Fougère, A., Jackson, A.P., Paraskevi Bechtsi, D., Braks, J.A.M., Annoura, T., Fonager, J., Spaccapelo, R., Ramesar, J., Chevalley-Maurel, S., Klop, O., et al. (2016). Variant Exported Blood-Stage Proteins Encoded by Plasmodium Multigene Families Are Expressed in Liver Stages Where They Are Exported into the Parasitophorous Vacuole. PLoS Pathog *12*, e1005917.

Fraschka, S.A., Filarsky, M., Hoo, R., Niederwieser, I., Yam, X.Y., Brancucci, N.M.B., Mohring, F., Mushunje, A.T., Huang, X., Christensen, P.R., et al. (2018). Comparative Heterochromatin Profiling Reveals Conserved and Unique Epigenome Signatures Linked to Adaptation and Development of Malaria Parasites. Cell Host Microbe *23*, 407–420.e408.

Garg, A., Lukk, T., Kumar, V., Choi, J.-Y., Augagneur, Y., Voelker, D.R., Nair, S., and Ben Mamoun, C. (2015). Structure, function and inhibition of the phosphoethanolamine methyltransferases of the human malaria parasites Plasmodium vivax and Plasmodium knowlesi. Sci. Rep. *5*, 9064–13.

Gulati, S., Ekland, E.H., Ruggles, K.V., Chan, R.B., Jayabalasingham, B., Zhou, B., Mantel, P.-Y., Lee, M.C.S., Spottiswoode, N., Coburn-Flynn, O., et al. (2015). Profiling the Essential Nature of Lipid Metabolism in Asexual Blood and Gametocyte Stages of Plasmodium falciparum. Cell Host Microbe *18*, 371–381.

Hahne, F., and Ivanek, R. (2016). Visualizing genomic data using Gviz and bioconductor. In Methods in Molecular Biology, pp. 335–351.

Huber, W., Carey, V.J., Gentleman, R., Anders, S., Carlson, M., Carvalho, B.S., Bravo, H.C., Davis, S., Gatto, L., Girke, T., et al. (2015). Orchestrating high-throughput genomic analysis with Bioconductor. Nat Meth *12*, 115–121.

Joice, R., Nilsson, S.K., Montgomery, J., Dankwa, S., Egan, E., Morahan, B., Seydel, K.B., Bertuccini, L., Alano, P., Williamson, K.C., et al. (2014). Plasmodium falciparum transmission stages accumulate in the human bone marrow. Science Translational Medicine *6*, 244re5–244re5.

Josling, G.A., Russell, T.J., Venezia, J., Orchard, L., van Biljon, R., Painter, H.J., and Llinás, M. (2020). Dissecting the role of PfAP2-G in malaria gametocytogenesis. Nature Communications *11*, 1–13.

Kafsack, B.F.C., Rovira-Graells, N., Clark, T.G., Bancells, C., Crowley, V.M., Campino, S.G., Williams, A.E., Drought, L.G., Kwiatkowski, D.P., Baker, D.A., et al. (2014). A transcriptional switch underlies commitment to sexual development in malaria parasites. Nature *507*, 248–252.

Karmodiya, K., Pradhan, S.J., Joshi, B., Jangid, R., Reddy, P.C., and Galande, S. (2015). A comprehensive epigenome map of Plasmodium falciparum reveals unique mechanisms of transcriptional regulation and identifies H3K36me2 as a global mark of gene suppression. Epigenetics & Chromatin *8*, 32.

Kent, R.S., Modrzynska, K.K., Cameron, R., Philip, N., Billker, O., and Waters, A.P. (2018). Inducible developmental reprogramming redefines commitment to sexual development in the malaria parasite Plasmodium berghei. Nat. Microbiol *3*, 1206–1213.

Kilian, N., Choi, J.-Y., Voelker, D.R., and Ben Mamoun, C. (2018). Role of phospholipid synthesis in the development and differentiation of malaria parasites in the blood. Journal of Biological Chemistry *293*, 17308–17316.

Lawrence, M., Huber, W., Pagès, H., Aboyoun, P., Carlson, M., Gentleman, R., Morgan, M.T., and Carey, V.J. (2013). Software for Computing and Annotating Genomic Ranges. PLoS Comput. Biol. *9*, e1003118.

Li, H., and Durbin, R. (2009). Fast and accurate short read alignment with Burrows-Wheeler transform. - PubMed - NCBI. Bioinformatics *25*, 1754–1760.

Li, H., Handsaker, B., Wysoker, A., Fennell, T., Ruan, J., Homer, N., Marth, G., Abecasis, G., Durbin, R., 1000 Genome Project Data Processing Subgroup (2009). The Sequence Alignment/Map format and SAMtools. Bioinformatics *25*, 2078–2079.

Li, S., Swanson, S.K., Gogol, M., Florens, L., Washburn, M.P., Workman, J.L., and Suganuma, T. (2015). Serine and SAM Responsive Complex SESAME Regulates Histone Modification Crosstalk by Sensing Cellular Metabolism. Molecular Cell *60*, 408–421.

Llorà-Batlle, O., Michel-Todó, L., Witmer, K., Toda, H., Fernandez-Becerra, C., Baum, J., and Cortés, A. (2020). Conditional expression of PfAP2-G for controlled massive sexual conversion in Plasmodium falciparum. Science Advances *6*, eaaz5057.

Lopez-Rubio, J.J., Mancio-Silva, L., and Scherf, A. (2009). Genome-wide analysis of heterochromatin associates clonally variant gene regulation with perinuclear repressive centers in malaria parasites. Cell Host Microbe *5*, 179–190.

Luo, M. (2018). Chemical and Biochemical Perspectives of Protein Lysine Methylation. Chem Rev *118*, 6656–6705.

McLean, K.J., Straimer, J., Hopp, C.S., Vega-Rodríguez, J., Small-Saunders, J.L., Kanatani, S., Tripathi, A., Mlambo, G., Dumoulin, P.C., Harris, C.T., et al. (2019). Generation of Transmission-Competent Human Malaria Parasites with Chromosomally-Integrated Fluorescent Reporters. Sci. Rep. *9*, 1–10.

Mentch, S.J., Mehrmohamadi, M., Huang, L., Liu, X., Gupta, D., Mattocks, D., Gómez Padilla, P., Ables, G., Bamman, M.M., Thalacker-Mercer, A.E., et al. (2015). Histone Methylation Dynamics and Gene Regulation Occur through the Sensing of One-Carbon Metabolism. Cell Metabolism *22*, 861–873.

Moll, K., Ljungström, I., Perlmann, H., and Scherf, A. (2008). Methods in malaria research. Manassas.

Neveu, G., Beri, D., and Kafsack, B.F. (2020a). Metabolic regulation of sexual commitment in Plasmodium falciparum. Curr Opin Microbiol *58*, 93–98.

Neveu, G., Richard, C., Dupuy, F., Behera, P., Volpe, F., Subramani, P.A., Marcel-Zerrougui, B., Vallin, P., Andrieu, M., Minz, A.M., et al. (2020b). Plasmodium falciparum sexual parasites develop in human erythroblasts and affect erythropoiesis. Blood *136*, 1381–1393.

Otto, T.D., Böhme, U., Jackson, A.P., Hunt, M., Franke-Fayard, B., Hoeijmakers, W.A.M., Religa, A.A., Robertson, L., Sanders, M., Ogun, S.A., et al. (2014). A comprehensive evaluation of rodent malaria parasite genomes and gene expression. BMC Biol *12*, 359.

Pollitt, L.C., Mideo, N., Drew, D.R., Schneider, P., Colegrave, N., and Reece, S.E. (2011). Competition and the evolution of reproductive restraint in malaria parasites. The American Naturalist *177*, 358–367.

Poran, A., Nötzel, C., Aly, O., Mencia-Trinchant, N., Harris, C.T., Guzman, M.L., Hassane, D.C., Elemento, O., and Kafsack, B.F.C. (2017). Single-cell RNA sequencing reveals a signature of sexual commitment in malaria parasites. Nature *551*, 95–99.

Prommana, P., Uthaipibull, C., Wongsombat, C., Kamchonwongpaisan, S., Yuthavong, Y., Knuepfer, E., Holder, A.A., and Shaw, P.J. (2013). Inducible Knockdown of Plasmodium Gene Expression Using the glmS Ribozyme. PLoS ONE *8*, e73783.

Quinlan, A.R., and Hall, I.M. (2010). BEDTools: a flexible suite of utilities for comparing genomic features. Bioinformatics *26*, 841–842.

Reguera, R.M., Redondo, C.M., Pérez-Pertejo, Y., and Balaña-Fouce, R. (2007). S-Adenosylmethionine in protozoan parasites: functions, synthesis and regulation. Mol Biochem Parasitol *152*, 1–10.

Salcedo-Amaya, A.M., van Driel, M.A., Alako, B.T., Trelle, M.B., van den Elzen, A.M.G., Cohen, A.M., Janssen-Megens, E.M., van de Vegte-Bolmer, M., Selzer, R.R., Iniguez, A.L., et al. (2009). Dynamic histone H3 epigenome marking during the intraerythrocytic cycle of Plasmodium falciparum. Proceedings of the National Academy of Sciences *106*, 9655–9660.

Shyh-Chang, N., Locasale, J.W., Lyssiotis, C.A., Zheng, Y., Teo, R.Y., Ratanasirintrawoot, S., Zhang, J., Onder, T., Unternaehrer, J.J., Zhu, H., et al. (2013). Influence of threonine metabolism on S-adenosylmethionine and histone methylation. Science *339*, 222–226.

Sinha, A., Hughes, K.R., Modrzynska, K.K., Otto, T.D., Pfander, C., Dickens, N.J., Religa, A.A., Bushell, E., Graham, A.L., Cameron, R., et al. (2014). A cascade of DNA-binding proteins for sexual commitment and development in Plasmodium. Nature *507*, 253–257.

Skene, P.J., Henikoff, J.G., and Henikoff, S. (2018). Targeted in situ genome-wide profiling with high efficiency for low cell numbers. Nature Protocols *13*, 1006–1019.

Sutter, B.M., Wu, X., Laxman, S., and Tu, B.P. (2013). Methionine inhibits autophagy and promotes growth by inducing the SAM-responsive methylation of PP2A. Cell *154*, 403–415.

Tibúrcio, M., Niang, M., Deplaine, G., Perrot, S., Bischoff, E., Ndour, P.A., Silvestrini, F., Khattab, A., Milon, G., David, P.H., et al. (2012). A switch in infected erythrocyte deformability at the maturation and blood circulation of Plasmodium falciparum transmission stages. Blood *119*, e172–e180.

Venugopal, K., Hentzschel, F., Valkiūnas, G., and Marti, M. (2020). Plasmodium asexual growth and sexual development in the haematopoietic niche of the host. Nat Rev Micro *18*, 177–189.

Warrenfeltz, S., Basenko, E.Y., Crouch, K., Harb, O.S., Kissinger, J.C., Roos, D.S., Shanmugasundram, A., and Silva-Franco, F. (2018). EuPathDB: The Eukaryotic Pathogen Genomics Database Resource. Methods Mol Biol *1757*, 69–113.

Wein, S., Ghezal, S., Bure, C., Maynadier, M., Perigaud, C., Vial, H.J., Lefebvre-Tournier, I., Wengelnik, K., and Cerdan, R. (2018). Contribution of the precursors and interplay of the pathways in the phospholipid metabolism of the malaria parasite. J. Lipid Res. *59*, 1461–1471.

Witola, W.H., and Ben Mamoun, C. (2007). Choline induces transcriptional repression and proteasomal degradation of the malarial phosphoethanolamine methyltransferase. Eukaryotic Cell *6*, 1618–1624.

Witola, W.H., Bissati, El, K., Pessi, G., Xie, C., Roepe, P.D., and Mamoun, C.B. (2008). Disruption of the Plasmodium falciparum PfPMT gene results in a complete loss of phosphatidylcholine biosynthesis via the serine-decarboxylase-phosphoethanolamine-methyltransferase pathway and severe growth and survival defects. J Biol Chem *283*, 27636–27643.

Ye, C., Sutter, B.M., Wang, Y., Kuang, Z., and Tu, B.P. (2017). A Metabolic Function for Phospholipid and Histone Methylation. Molecular Cell *66*, 180–193.e188.

Ye, C., Sutter, B.M., Wang, Y., Kuang, Z., Zhao, X., Yu, Y., and Tu, B.P. (2019). Demethylation of the Protein Phosphatase PP2A Promotes Demethylation of Histones to Enable Their Function as a Methyl Group Sink. Molecular Cell *73*, 1115–1126.e1116.

Zhang, Y., Liu, T., Meyer, C.A., Eeckhoute, J., Johnson, D.S., Bernstein, B.E., Nussbaum, C., Myers, R.M., Brown, M., Li, W., et al. (2008). Model-based analysis of ChIP-Seq (MACS). Genome Biol *9*, R137.

SUPPLEMENTARY FIGURES:

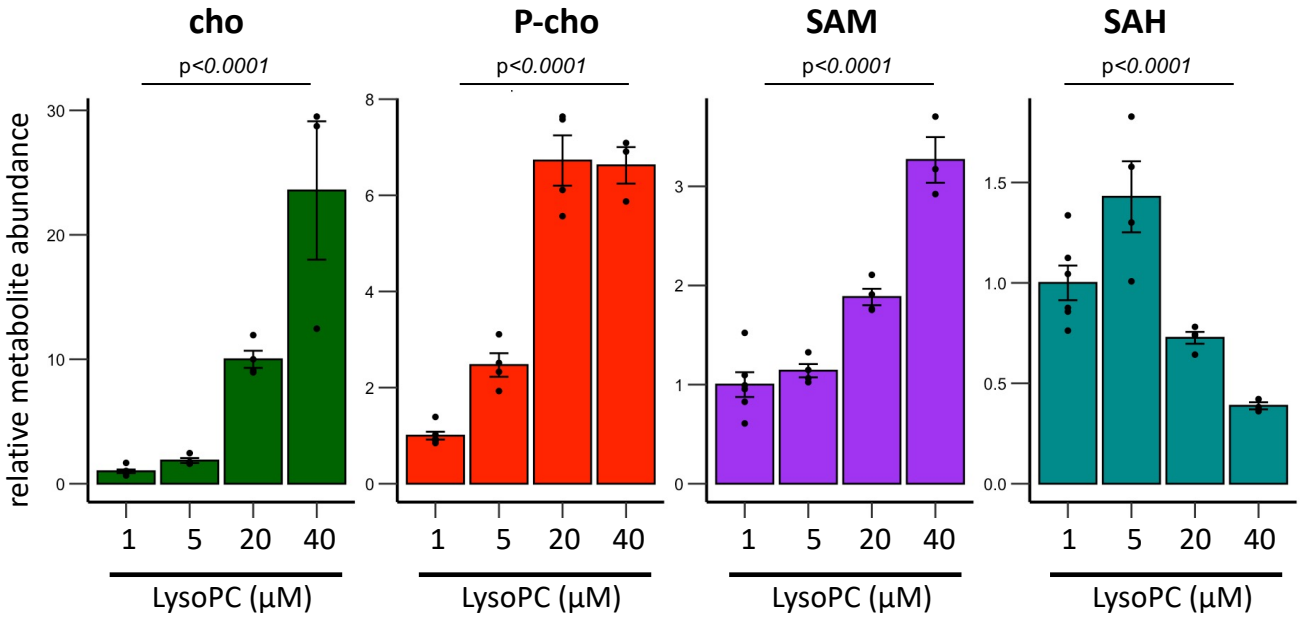

Figure S1: Dose-dependent metabolic response to LysoPC.
Parasites were cultured in media spiked with increasing concentrations of LysoPC. Bar graphs show the mean intracellular metabolite abundances per thousand parasites ± s.e.m (n=3-5). Italicized numbers are p-values based on two-sided ANOVA tests.

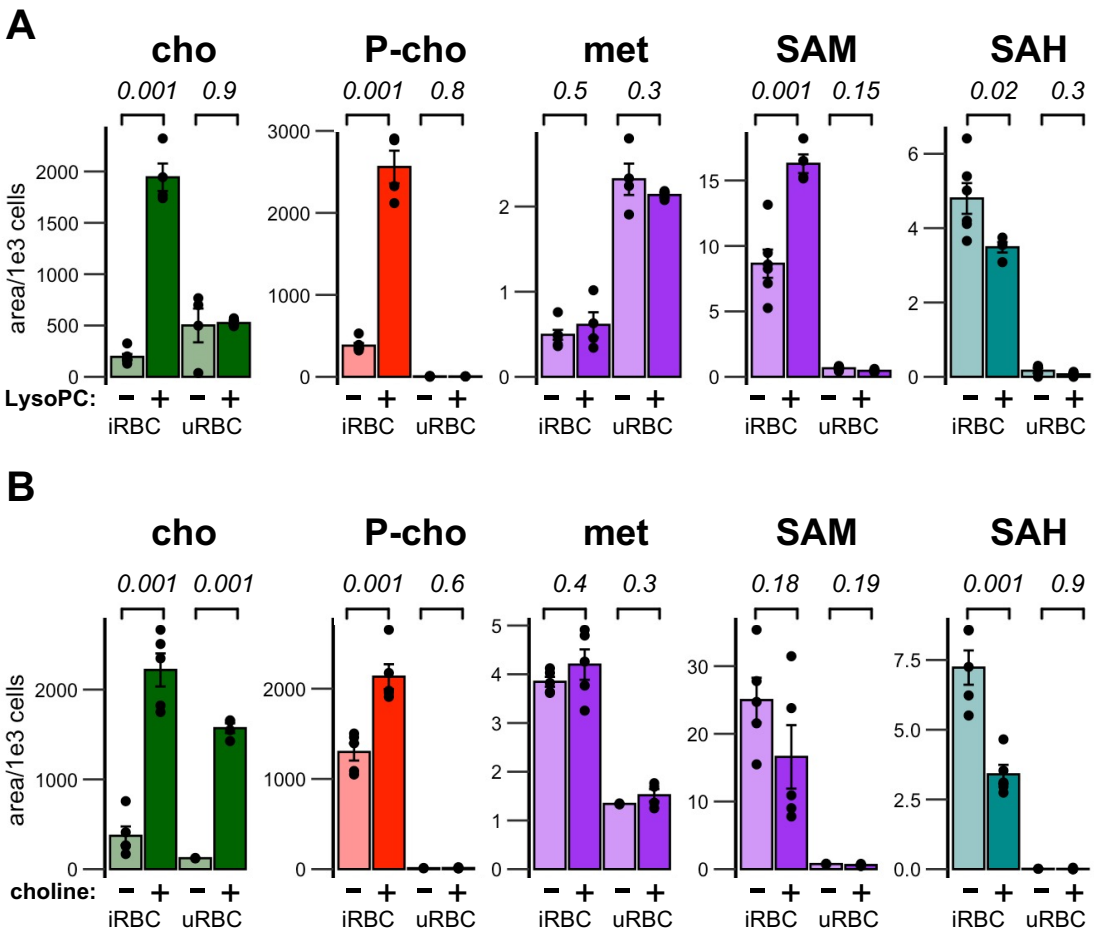

Figure S2: Changes in SAM/SAH metabolism are specific to parasite metabolism.
LCMS quantification of indicted metabolites. Infected and uninfected cultures were cultured in the presence or absence of 20 µM LysoPC or 420µM choline for ~36 hpi during the commitment cycle. Infected (iRBC) and uninfected (uRBC) erythrocytes were then extracted, and metabolite abundances were quantified by LCMS. Bar graphs show the mean intracellular metabolite abundances per thousand cells ± s.e.m (n=3-5). Italicized numbers are p-values based on two-sided paired t-tests.

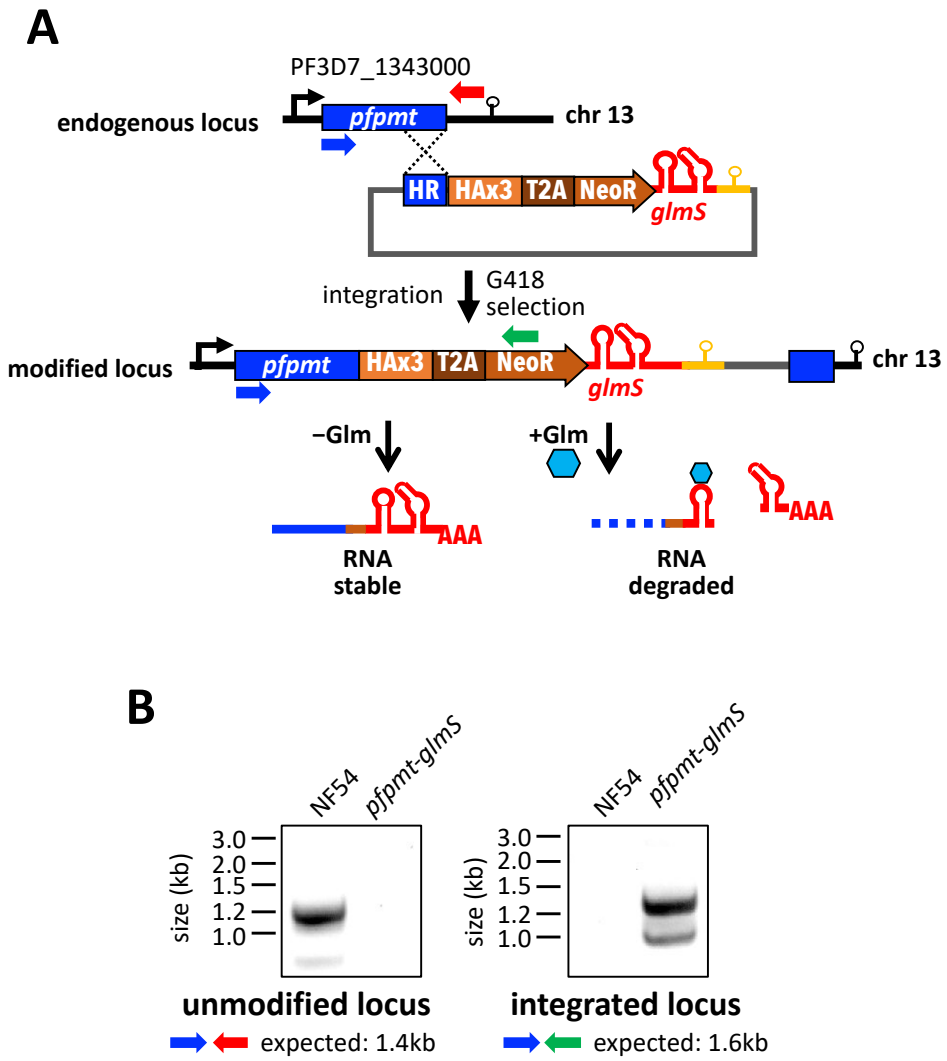

Figure S3: Validation of *pfpmt-glmS* knockdown parasite line.
(A) Generation of *pfpmt-glmS* knockdown parasites by selection-linked integration. **(B)** Validation PCR demonstrating tagging of the endogenous *pfpmt* locus.

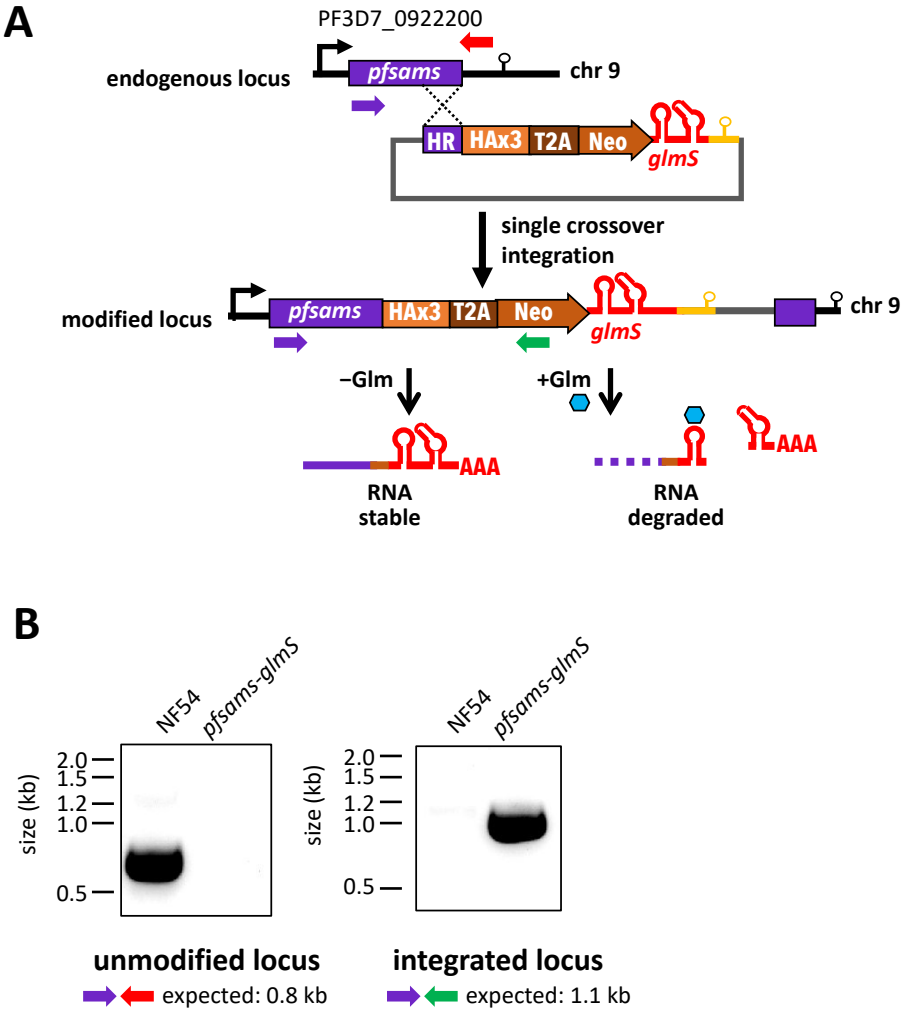

Figure S4: Validation of *pfsams-glmS* knockdown parasite line.
(A) Generation of *pfsams-glmS* knockdown parasites by selection-linked integration. **(B)** PCR Validation demonstrating tagging of the endogenous *pfsams* locus.

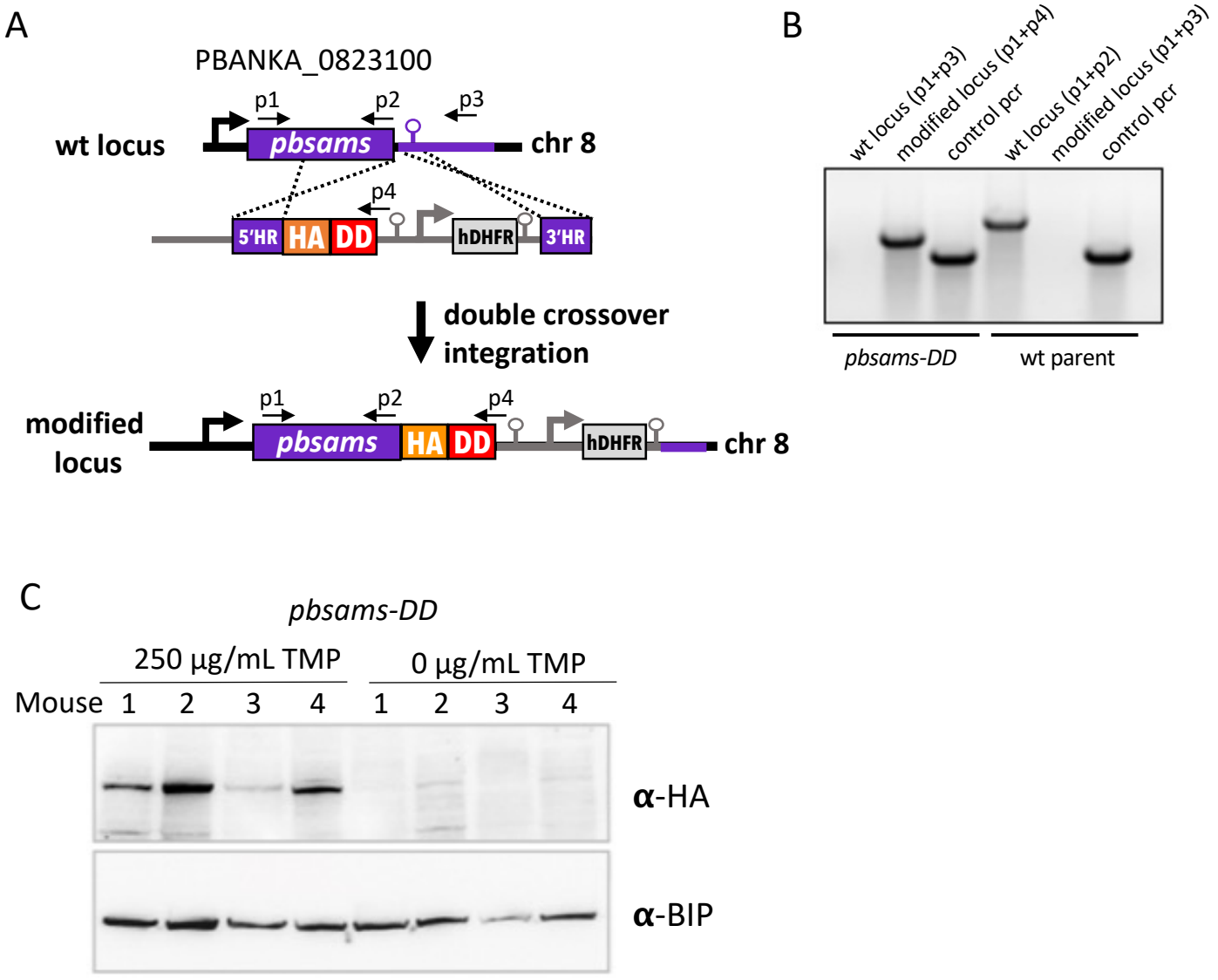

Figure S5: Validation of *pbsams-DD* knockdown parasite line.
(A) The endogenous *pbsams* locus in the *P. berghei* ANKA strain background was modified by homologous integration to add the ecDHFR destabilization domain (DD) and hemagglutinin epitope tag (HA) at the 3' end of the *pbsams* coding sequence. Simultaneous integration of a hDHFR expression cassette allows for selection of integrants. **(B)** PCR validation of successful tagging in *Pb*SAMS-DD-HA parasites. **(C)** Successful knockdown of *Pb*SAMS upon removal of trimethoprim (TMP) from the drinking water in mice infected with *pbsams-DD* parasites**.** Parasite lysates were assayed for the abundance of *Pb*SAMS-DD with antibodies against the HA epitope tag and *Pb*BIP, which served as a loading control and was used for normalization.

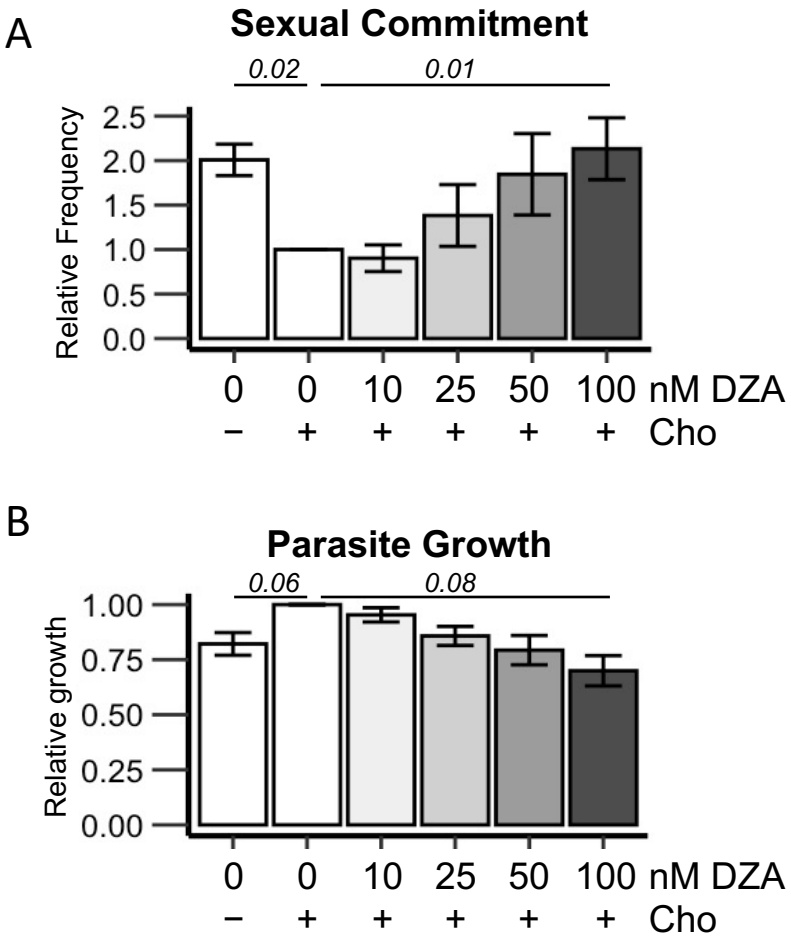

Figure S6: Dose-response of parasite sexual commitment (A) and growth (B) to 3-DZA.
Italicized number is the p-value based on a two-sided t-tests for the +/- choline comparison and ANOVA for the DZA dose response (n=4).

Table S1: Compositions of cell culture media used in this study.

Label	Differences to standard malaria complete media
- cho	0 µM choline
+ cho	420 µM Choline
- LysoPC	30 µM Palmitate, 30 µM oleate, 1.25 µM LysoPC, 4 g/L Fatty Acid Free BSA, no Albumax II,
+ LysoPC	30 µM Palmitate, 30 µM oleate, 40 µM LysoPC, 4 g/L Fatty Acid Free BSA, no Albumax II,
- Glm	none
+ Glm	2.5mM glucosamine
- met	0 µM methionine
+ met	none (100 µM methionine)
- 3DZA	420 µM Choline
+ 3DZA	420 µM Choline, 100nM 3-DZA

Table S2: Primers used in this study

PrimerID	Sequence	Strand	Purpose
BKO-1424	TATGCTGATATTCTTACTGCTTGC	F	qRT-PCR for *pfpmt* transcript
BKO-1425	GGACCAGCCATCATCAAGAC	R	qRT-PCR for *pfpmt* transcript
BKO-1626	AAGTAGCAGGTCATCGTGGTT	F	qRT-PCR for serine t-RNA ligase
BKO-1627	TTCGGCACATTCTTCCATAA	R	qRT-PCR for serine t-RNA ligase
BKO-1004	ctatagaatactcaagctgcggccgcGGAGCACATACTCACGGTATAGAT	F	for cloning *pfpmt* homology block for *pfpmt-glmS* tagged line
BKO-1005	ccgggacgtcgtacgggtacccgggATTTTTGGTGGCCTTAAAATAACC	R	for cloning *pfpmt* homology block for *pfpmt-glmS* tagged line
BKO-1002	ctatagaatactcaagctgcggccgcCCTTTACGTGTTCATACTGTTCTTATT	F	for cloning *pfsams* homology block for *pfsams-glmS* tagged line
BKO-1003	ccgggacgtcgtacgggtacccgggATTTTTTAATGCATTTTTTTCGTG	R	for cloning *pfsams* homology block for *pfsams-glmS* tagged line
BKO-0750	TGACTTTGATTGAAAACTTAAACTCTG	F	PCR verification *of pfpmt-glmS* line; binds within *pfpmt* CDS upstream of homology region
BKO-1661	CTGCATATTATGCATCGGGATAC	R	PCR verification of *pfpmt-glmS line* ; binds within *pfpmt* 3' UTR
BKO-1023	GTATCTTACCTTATTTAGGACCTGATG	F	PCR verification of *pfsams*-glmS; binds in *pfsams* CDS upstream of homology region
BKO-1009	ACATTTCTTCTTTCTCATTCCTAAAT	R	PCR verification of genome editing; binds within *pfsams* 3' UTR
BKO-0217	AGTGACAACGTCGAGCACAG	R	PCR verification of *pfpmt-glmS* & *pfsams-glmS* lines; binds within the neomycin resistance gene
P1	taggtaccGAGGAAATTTTCTATTTACTTCG	F	Validation of *pbsams-dd-ha* parasites, binds within *pbsams* CDS upstream of homology region
P2	tagggcccATTTTTTAAAACATTTTTTTCGTG	R	Validation of *pbsams-dd-ha* parasites, binds at 3' end of *pbsams* CDS, used as a PCR positive control
P3	atgcggccgcCAACTAATAAAATCCAGGAAATA	R	Validation of *pbsams-dd-ha* parasites, binds within *pbsams* 3'UTR, downstream of the 3' homology region
P4	taGCGGCCGCTCATCGCCGCTCCAGAATCTC	R	Validation of *pbsams-dd-ha* parasites, binds within the DD CDS sequence

Upper case letters indicate the annealing region matching the template